NASA CONTRACTOR REPORT

NASA CR-609

NASA CR-609



# PEAK PRESSURES IN THICK TARGETS GENERATED BY REDUCED DENSITY PROJECTILES

*by J. E. Heyda and T. D. Riney*

*Prepared by*
GENERAL ELECTRIC COMPANY
Philadelphia, Pa.
*for Lewis Research Center*



NATIONAL AERONAUTICS AND SPACE ADMINISTRATION • WASHINGTON, D. C. • SEPTEMBER 1966

NASA CR-609

# PEAK PRESSURES IN THICK TARGETS GENERATED BY REDUCED DENSITY PROJECTILES

By J. F. Heyda and T. D. Riney



Prepared under Contract No. NAS 3-4176 by
GENERAL ELECTRIC COMPANY
Philadelphia, Pa.

for Lewis Research Center

NATIONAL AERONAUTICS AND SPACE ADMINISTRATION

For sale by the Clearinghouse for Federal Scientific and Technical Information
Springfield, Virginia 22151 – Price $2.00

## FOREWORD

The work described herein was sponsored by the National Aeronautics and Space Administration, Lewis Research Center, under Contract NAS 3-4176. Technical direction for the Lewis Research Center was provided by Jack F. Mondt of the Space Power Systems Division and Irvin J. Loeffler of the Airbreathing Engines Division.

## ABSTRACT

This report presents an analytical formulation for evaluating peak pressures in thick targets impacted by hypervelocity projectiles of subnormal bulk densities at normal incidence. The formulation gives good agreement with available hydrodynamic computer program (PICWICK) calculations for describing peak pressure propagation. Calculations are made for an aluminum target impacted by reduced density aluminum projectiles of densities 2.702, 0.9, 0.44, 0.2 and 0.1 gm/cc.

# PEAK PRESSURES IN THICK TARGETS GENERATED BY REDUCED DENSITY PROJECTILES

by J. F. Heyda and T. D. Riney

General Electric Space Sciences Laboratory

## SUMMARY

An existing analytical method for calculating peak pressures in thick targets impacted by end-on oriented cylindrical projectiles of like material at hypervelocities is extended to cover the case of projectiles of subnormal bulk density. Projectiles and target are assumed to be of aluminum. Projectile densities assumed in the study are 2.702, 0.9, 0.44, 0.2 and 0.1 gm/cc. Two impact velocities are considered, 20 km/sec and 7.6 km/sec.

It is shown that the method gives good agreement with computer program (PICWICK) calculations which evaluate numerically the hydrodynamic phase of impact at 20 km/sec with projectiles of densities 2.702, 0.9 and 0.44 gm/cc. The method is then employed to investigate impacts at the lower densities, 0.2 and 0.1 gm/cc, and at the two impact velocities, 20 km/sec and 7.6 km/sec in order to investigate variation in peak axial pressure propagating into the target as a function of projectile density.

At 20 km/sec it was found that projectiles of the same mass but of differing densities will give essentially equivalent peak pressure profiles in the target for densities as low as 0.44 gm/cc. This is still true at 7.6 km/sec providing the projectile densities are greater than some limiting density above 0.9 gm/cc.

The calculated initial peak pressures at the target surface at impact are greater for the higher density projectiles for equal projectile mass and velocity. However, after the shock has progressed well into the target, the peak axial pressure of the decaying shock for low density projectiles of 0.1 and 0.2 gm/cc density exceeds that for higher density projectiles (0.44 gm/cc and greater). This conclusion does not take into account strain-rate and strength effects in the target flow field and hence must remain tentative until supported by detailed computer program calculations that include these effects. The analytical model used in making the pressure profile calculations is strongly dependent on the form of the Hugoniot function used for the subnormal density projectile material. Thus, the conclusion is considered tentative until supported by an appropriate sensitivity study.

# INTRODUCTION

The operation of a space waste-heat radiator, as well as some other spacecraft components, involves the rather lengthy exposure of large vulnerable areas to meteoroid bombardment in space. The possible severe weight penalty associated with the armor or other protective material for these devices requires that realistic damage relations be determined to permit the development of efficient, lightweight meteoroid protection.

In the evaluation of the meteoroid hazard to space vehicles, an important area of uncertainty is the effect of the physical characteristics of the meteoroid on its penetrating ability. The majority of the meteoroids important to large components such as space radiators appear to be of heterogeneous, porous structure of low average bulk density around 0.2 gm/cc (ref. 1). At present, no experimental data are available concerning the impact of heterogeneous projectiles of such low densities even at the lower limit of the velocity range of interest, 7.6 km/sec. It has been speculated that impact damage resulting from such particles might not be the same as from solid particles of the same mass (ref. 2).

Laboratory acceleration devices are currently unable to achieve the typical meteoroid velocities of 20 to 30 km/sec even with well defined solid projectiles. The laboratory simulation of hypervelocity impact by heterogeneous low-density fluffy projectiles appears well beyond the present state of the art.

In view of the limited capability of experimental techniques in simulating hypervelocity impact by heterogeneous low-density meteoroid particles, the Flow Analysis Branch of the Lewis Research Center has recognized the desirability of employing theoretical techniques in the investigation of this problem.

Theoretical impact programs using high speed computers have been developed to study the cratering of metal targets subjected to impact by subnormal density projectiles of either homogeneous or heterogeneous structure. The programs, designated PICWICK, have been developed to solve the system of equations governing the visco-plastic model which accounts for the inertial, strain-rate and strength effects in the cratering process (ref. 3). When the strain-rate and strength effects are neglected, the model reduces to the hydrodynamic model. The original version of the code, PICWICK I, employed a particle-in-cell numerical scheme and utilized only the internal memory of the IBM 7094. A later version, PICWICK II, employs the same basic numerical scheme as PICWICK I but utilizes external tape memory to permit a larger number of cells in the computational mesh. In PICWICK III the discrete mass point representation of the material in the second phase of the calculations is replaced by a continuous mass representation. It is a purely

Eulerian scheme and permits over 2200 computational cells using internal storage only.

In the late stages of the cratering process it has been found that the particle-in-cell scheme does not give sufficient resolution of the flow process because of the discrete nature of the mass representation. The continuous mass representation used in PICWICK III is thus best suited for following the flow when the pressure pulse has attenuated to the point that the strength and strain-rate effects predominate. On the other hand, a heterogeneous projectile configuration can best be described by the particle-in-cell scheme. Consequently, the numerical calculations will use PICWICK II to study the early stages of the flow process until the projectile has buried itself into the target. At this point the field variables will be read out on tape and used for initial data for subsequent PICWICK III calculations which will continue until, hopefully, strength and strain-rate effects stop the flow process.

Even in the particle-in-cell representation, the mass distribution within each cell used to describe the projectile material is assumed to be of uniform density. Within each cell, therefore, the method treats the projectile material as homogeneous and heterogeneity occurs only in the cell-to-cell variations. A projectile material with a large number of very small pores would necessarily be treated as a homogeneous sub-normal density material. At the other extreme, the projectile material may have no pores and would be represented by a homogeneous material of normal density.

In carrying out computer calculations with PICWICK I in earlier studies (ref. 4), it was found that the local values of the pressure obtained fluctuated about the true values of the pressure due to the discrete nature of the difference scheme employed in the program and to the fact that the pressure is independently calculated at each time cycle. On the other hand, the calculated values of the velocity and momentum components are more accurate since their values are obtained by integrating the incremental changes over all the preceding time steps.

Fluctuations in the pressure computed from PICWICK I give rise, for example, to a polygonal peak axial pressure-versus-distance profile in the target which weaves itself about the true profile. Such fluctuation makes it difficult to compare the response of a target to distinct impact situations involving, for example, projectiles of differing densities but of equal mass and speed. To effect such a comparison would require a better resolution of the pressure pulse and its variation with distance. To this end an existing analytical model for determining peak axial pressure in a thick target (ref. 5) has been extended to treat impact by projectiles of subnormal bulk density. The model considers the projectile to be homogeneous and thus treats the limiting case of many small pores and, for normal bulk density, the case of no pores. It furnishes a continuous curve of peak axial pressure as a function of shock penetration along the axis of symmetry for arbitrary impact speed of a right

circular cylindrical projectile of arbitrary aspect ratio and density. Although the model assumes hydrodynamic flow, it is nevertheless useful in giving a preliminary indication of how reduced projectile density affects pressure decay in the target. Thus we shall see that for impact speeds from 7.6 to 20 km/sec, two projectiles of the same mass and speed but with densities of 0.44 and 0.2 gm/cc produce noticeably different pressure profiles in a thick target. It should be stated that the analytical model is based partly on theoretical considerations and partly on empirical deductions from smoothed PICWICK I computer program calculations and as such can be used to predict peak axial pressures independently of additional computer runs.

The inputs to the analytical model involve: projectile shape, speed and density; undisturbed target density and speed of sound; the Hugoniot values of the pressure, density, sound and shock speeds in the target at impact; and several parameters derivable from them. In the next section we review and formulate the model in detail.

Since the Hugoniot values depend on the equations of state employed for projectile and target materials, a separate section of the report is devoted to equations of state and a method for making Hugoniot calculations is outlined. Results of such calculations are displayed both tabularly and graphically.

The succeeding section presents the results of applying the model to specific impact situations involving normal and subnormal density aluminum projectiles and a normal density aluminum target. PICWICK I computer program calculations are also displayed for comparison.

Conclusions which follow from a study of these impact situations are then given along with a general discussion of the results. This is followed by a list of specific references to material cited earlier in the text.

## ANALYTICAL MODEL

In this section there is presented a detailed description of the analytical model for determining the peak pressure back of the shock as it propagates in the target after impact. Part A treats the case when the impacting projectile is of normal density; part B gives the extension of the model required for projectiles of subnormal bulk density.

### A. Normal Density Projectiles

Consider the hypervelocity impact at speed $V_o$ of a right circular cylindrical projectile of radius L and length $\ell$ at normal incidence into a thick target. (Fig. 1. Definitions of symbols are given in Appendix A). For a short time $t_1$ after impact the peak pressure of the pulse propagating into the target will remain constant at the impact Hugoniot value $p_i$ and the speed of propagation $\dot{R}_i$ will also be constant. In the immediate vicinity of the axis of penetration into the target the shock front will be planar and the target material between it and the moving projectile-target interface will be a region of unattenuated pressure $p_i$. Immediately after impact this region begins to be relaxed by a rarefaction front originating at the projectile periphery. This front eventually attenuates the peak pressure on the axis at the point $R_1$ at time $t_1$ since impact, where $R_1 = \dot{R}_i t_1$ (see Fig. 1(a) where the situation in the projectile material is also indicated). At a time $t_i < t_1$ the rarefaction fronts will be tangent to the axis and the region of unrelaxed pressure $p_i$ in target and projectile is actually separated into two parts (see Fig. 1(b) ). As shown in reference 4 the point $R_1$ is located below the original target surface at a distance equal to

$$R_1 = \frac{\dot{R}_i L}{\left[c_i^2 - x_i^2 \dot{R}_i^2\right]^{1/2}} , \qquad (1)$$

where $x_i = \rho_o / \rho_i$ is the compression ratio across the shock moving into the target and $c_i$ is the speed of the rarefaction front in the moving pressurized material. Here $\rho_o$ is the undisturbed target density and $\rho_i$ is the density behind the shock at impact.

Once the pressure pulse along the axis has passed the point $R_1$ a rapid decline in its peak value and speed of propagation occurs. At an axial position $R > R_1$ the peak value p is determined from the Hugoniot function p(x), where $x = \rho_o / \rho$ and $\rho$ is the density behind the shock at this position. The speed of the shock at position R may also be obtained as a function of x. Denoting it by $\dot{R}$ we find from the Rankine-Hugoniot relations for the conservation of momentum and mass across the shock that

$$p = \rho_o \dot{R} u \quad , \quad \rho_o \dot{R} = \rho(\dot{R} - u) \quad ,$$

where u is the particle velocity behind the shock. [Velocities $\dot{R}$ and u are taken with respect to the original target surface.] Eliminating u then yields the result

$$\dot{R} = \sqrt{\frac{p(x)}{\rho_o(1 - x)}} \quad . \tag{2}$$

The peak pressure p as a function of R requires knowledge of $\dot{R}$ as a function of R. No exact theoretical relationship giving axial shock propagation speed as a function of position is known at this time. The relationship adopted here is based on the following heuristic considerations. When the rarefaction fronts reach $R_1$ there is an intense energy release along the axial direction which occurs in a very short time interval and approximates a line blast. The shock front, moving as a planar front for $R < R_1$, is assumed to have, subsequent to the energy release, a speed equal to that of a planar blast wave. This assumption is made in order to account for the strong axial gradient in the energy dissipation along the axis. However, the line blast effect diminishes the planar blast wave speed by an amount that is proportional to the speed of a cylindrically radial front. To follow this empirical reasoning we denote in Figure 2 the arc PG as a small section of the actual shock front adjacent to the axis an instant after the front has passed $R_1$. If there were no energy release on the axis this front would be planar and along GC. From the figure we note that for $\theta$ very small,

$$\begin{aligned} \mathcal{R} = OP &= OC - PC \\ &= OG \sec\theta - DE \\ &\doteq OG - FP \\ &= R - \bar{R} \sin\theta, \qquad (R = OG) \quad . \end{aligned}$$

Hence, the front speed in direction $\theta$ is

$$\dot{\mathcal{R}} = \dot{R} - \dot{\bar{R}} \sin\theta, \tag{3}$$

which gives the decomposition into planar blast wave speed $\dot{R}$ and cylindrical blast wave speed $\dot{\bar{R}}$. Now it is known from blast wave theory that

$$\dot{R} = B\Big/\sqrt{R - R_o} \quad , \qquad \dot{\bar{R}} = D/\bar{R} = D/\mathcal{R} \sin\theta \quad , \tag{4}$$

where $R_o$ is the effective center and B and D are constants. Combining (3) and (4) and letting $\theta \to 0$ gives the axial shock front speed as

$$\dot{R} = \frac{B}{\sqrt{R - R_o}} - \frac{D}{R - R_o} \quad , \qquad R \geq R_1 \quad . \tag{5}$$

For convenience we introduce new constants A, k which are related to B and D by

$$k = \frac{D}{B} \quad , \qquad A = \frac{B}{4k} \tag{6}$$

and rewrite (5) as

$$\dot{R} = A \left[ \frac{4k}{\sqrt{R - R_o}} - \frac{4k^2}{R - R_o} \right] \quad , \qquad R \geq R_1 \tag{7}$$

Relation (7) supplies $\dot{R}$ as a function of R and combined with (2) will furnish the peak axial pressure in terms of axial position R. For plotting p in terms of R it is convenient to take x as the independent variable. Using it we get p from $p = p(x)$ and $\dot{R}$ from (2) and (7), whence one plots p vs R.

To determine the axial pressure profile in a specific case one must know the values of the parameters A, k, $R_o$. The parameter A, which has dimensions of a velocity, may be determined by requiring the profile to have a point of inflection at $R = R_1$. In actuality it has a corner there; little is lost, however, if one approximates the physical process by a continuous curve with a continuous slope. In reference 5 it is shown that this assumption leads to an explicit determination of A in the form

$$A = \dot{R}_i f(\beta) \quad , \tag{8}$$

where $f(\beta)$ depends only on the material properties of the target:

$$f(\beta) = \frac{51 - 44\beta + 8\beta^2 - 3\sqrt{33 - 8\beta}}{8(1 - \beta)(4 - \beta)} \tag{9}$$

and $\beta$ is in turn computed from the formulas

$$\beta = 4d_1 \left(1 - \frac{d_1}{d_2}\right) \quad ,$$

$$d_1 = p_i \Big/ \left(p_i + [1 - x_i] p_i'\right) \quad , \tag{10}$$

$$d_2 = 2p_i' / (1 - x_i) p_i'' \quad ,$$

where $p_i' \equiv (dp/dx)_{x = x_i}$ , etc.

As $V_o$ ranges over all hypervelocities of interest, the dimensionless quantity $\beta$ varies from -1 to 0. The quantity $f(\beta)$ , however, exhibits variation beginning only with the third decimal place, being approximately 1.055.

The parameter $k^2$ has dimensions of a length and can be regarded as a measure of the average distance over which the line blast effect is operative. It is convenient for generality to consider k in non-dimensional form, namely

$$K = \frac{k}{\sqrt{\bar{L}}} \quad , \quad \bar{L} = (L^2 \ell)^{1/3} = L\left(\frac{\ell}{L}\right)^{1/3} \quad . \tag{11}$$

Once the dimensionless parameter K is known, k is then calculated from

$$k = K\sqrt{L}\left(\frac{\ell}{L}\right)^{1/6} \quad . \tag{12}$$

For determining K use was made of the hydrodynamic computer code program (PICWICK I) solutions of the partial differential equations describing the impact generated flow in the target. This was done in the following fashion (see reference 5 for a detailed report of the numerical work). Equation (7) was put into the non-dimensional form

$$\frac{R}{\bar{L}} = \frac{R_o}{\bar{L}} + \left[\frac{2K}{1 - \sqrt{1 - \frac{\dot{R}}{A}}}\right]^2 \tag{13}$$

in which, for a given impact situation, A is known from equations (8, 9, 10). At $R = R_1$ we require $\dot{R} = \dot{R}_i$; thus $\frac{R_o}{\bar{L}}$ can be evaluated from (13) by using this data point. We find

$$\frac{R}{\bar{L}} = \frac{R_1}{\bar{L}} + \left\{\left[\frac{2}{1 - \sqrt{1 - \frac{\dot{R}}{A}}}\right]^2 - \left[\frac{2}{1 - \sqrt{1 - \frac{\dot{R}_i}{A}}}\right]^2\right\} K^2 \quad . \tag{14}$$

For a selected impact situation $\frac{R_1}{\bar{L}}$ is computed with the aid of (1) and computer program data for the speed of peak pressure propagation along the axis then furnishes many $(R, \dot{R})$ points. K is then selected so that the $\dot{R}$ vs R curve defined by Equation (14) gives an optimum fit to the $(R, \dot{R})$ points of the computer program data.

From a study of the computer program computations for many individual impact cases for like-material impacts of aluminum, lead and iron it was determined that K has the form

$$K = \alpha V_o^{-1/3} \tag{15}$$

where $\alpha$ is a parameter characterizing the target material. The latter dependence is principally on the sound speed $c_o$ in the undisturbed material. In fact, it was found that

$$\alpha = 0.368\, c_o^{1/3} \quad , \tag{16}$$

so that K can be written as

$$K = 0.368 \left( \frac{V_o}{c_o} \right)^{-1/3} \quad , \tag{17}$$

where 0.368 is a dimensionless impact constant whose further identification must await future refinements of the theory.

With the determination of K, the remaining parameter $R_o$ is now known from equations (13, 14), namely

$$\frac{R_o}{\bar{L}} = \frac{R_1}{\bar{L}} - \left[ \frac{2K}{1 - \sqrt{1 - \frac{\dot{R}_i}{A}}} \right]^2 \quad . \tag{18}$$

The time of arrival t at an axial location R of the peak of the pressure pulse propagating in the axial direction in the target can be obtained by integrating the differential equation (13) and evaluating the constant of integration with the known data at point $R_1$. The result is

$$\frac{t}{\bar{L}} = \frac{R_1/\bar{L}}{\dot{R}_i} + \frac{1}{2AK} \left\{ \sum_{j=0}^{2} \frac{K^j}{3-j} \left( \frac{R - R_o}{\bar{L}} \right)^{\frac{3-j}{2}} + K^3 \ell n \left( \sqrt{\frac{R - R_o}{\bar{L}}} - K \right) - K^3 \left( \ell n K + \frac{20}{3} \right) \right\} \quad . \tag{19}$$

This completes the description of the analytical model in so far as impacts with normal density projectiles are concerned.

B. Subnormal Bulk Density Projectiles

To extend the model to be applicable to impacting projectiles of subnormal bulk density it is necessary to modify formula (17) for K. In addition an appropriate model is needed for the Hugoniot equation of state of the projectile material, $p = p(x)$. The selection of a realistic Hugoniot function $p(x)$ for a material of subnormal bulk density can be made to depend on the Hugoniot function of the corresponding normal density material. How this is done is considered in detail in the following section on Equations of State.

To determine K, computer program calculations using the PICWICK I code were made for impacts of subnormal bulk density aluminum projectiles into a thick normal density aluminum target at an impact velocity $V_o$ of 20 km/sec with projectile densities of 0.9 gm/cc and 0.44 gm/cc. For each case the projectile size was taken to be $L = \ell = 0.26192$ cm. In addition to these two subnormal density cases there is also available the computer program data for a normal density projectile of the same size and speed from the work presented in reference 5. On the basis of these PICWICK I calculations for impacts at 20 km/sec of aluminum projectiles of densities 2.702, 0.9, 0.44 gm/cc into normal density aluminum, a density factor was deduced for inclusion in formula (17) for K given by

$$1 + 0.15\,(1 - \delta) \quad , \tag{20}$$

where $\delta$ = subnormal density/normal density. The modified formula for K is therefore

$$K = 0.368\,[1 + 0.15\,(1 - \delta\,]\left(\frac{V_o}{c_o}\right)^{-1/3} \tag{21}$$

It is of some interest to speculate on the meaning of the factor (20). As was pointed out in reference 4 the impact generated flow is an energy dependent process and one would expect the dimensionless parameter K to involve the specific projectile energy $E = \frac{1}{2}\,\rho_P\,V_o^2$, where $\rho_P$ is the density of the undisturbed projectile material. A natural scaling factor here is $\rho_T\,c_o^2$, where $\rho_T$ and $c_o$ are the density and sound speed of the undisturbed target material. The ratio may be written as

$$\frac{E}{\rho_T\,c_o^2} = \frac{1}{2}\,\frac{\rho_P}{\rho_T}\left(\frac{V_o}{c_o}\right)^2 = \frac{1}{2}\,\delta\left(\frac{V_o}{c_o}\right)^2 \quad ,$$

whence

$$\left(\frac{E}{\rho_T c_o^2}\right)^{-1/6} = 2^{1/6}\,\delta^{-1/6}\left(\frac{V_o}{c_o}\right)^{-1/3}$$

In view of (21) one would expect then that

$$K = (\text{const})\left(\frac{E}{\rho_T c_o^2}\right)^{-1/6} \tag{22}$$

with the identifications

$$\text{const} = \frac{.368}{6\sqrt{2}} = 0.328 \quad ,$$

$$\delta^{-1/6} \approx 1 + 0.15(1 - \delta) \tag{23}$$

The right member of (23), obtained by strictly empirical calculations, suggests the first two terms of the binomial expansion of

$$\delta^{-1/6} \equiv \left[1 + (\delta - 1)\right]^{-1/6} = 1 + \frac{1}{6}(1 - \delta) + \cdots \quad .$$

These manipulations would appear then to indicate that (21) is an approximation to the form of K given by (22). In the present study the form (21) will be used, however, since it is based on direct computer program calculations.

Employing (21) and an appropriate Hugoniot function p(x) for the projectile material one can now compute peak axial pressure profiles in the target, as outlined in part A, for projectile impacts of arbitrary subnormal density projectiles. It should be emphasized that the profiles obtained will be strongly dependent on the specific Hugoniot function p(x) adopted for the projectile material. The sensitivity of these profiles to a change in the form of the Hugoniot function is not, however, investigated in this report. Owing to the complexity of other possible forms of the Hugoniot function such an investigation would involve extensive computations which would more properly form the substance of a separate report.

## EQUATIONS OF STATE

In the computer program calculations for impact generated flow in the target, the equation of state employed is that due to the research group at Los Alamos (ref. 6). For a material of normal density $\rho_o$ this equation expresses the pressure p as a function of density $\rho$ and the internal energy I per unit mass,

$$p = f(\rho, I) \tag{24}$$

where

$$f(\rho, I) = \frac{1}{\Phi + \Phi_o}\left[\zeta\left(a_1 + a_2|\zeta|\right) + \Phi\left|b_o + \zeta(b_1 + b_2\zeta) + \Phi(c_o + c_1\zeta)\right|\right],$$

$$\zeta = \frac{\rho}{\rho_o} - 1 \quad , \quad \Phi = \rho_o I \quad , \quad \zeta \geq -1 \quad , \tag{25}$$

and the coefficients $a_1$, $a_2$, $b_o$, $b_1$, $b_2$, $c_o$, $c_1$, $\phi_o$ are constants whose values are specified for a given material. Values of these constants are given for several metals in reference 5. Their specific values for aluminum in the gm-cm-$\mu$sec system of units appears in Appendix B.

The analytical model described in the preceding section employs Hugoniot functions for both target and projectile. The Hugoniot function p(x) for the target material (normal density aluminum) is obtained in the usual manner by replacing I in (24) by

$$I = \frac{p}{2}\left(\frac{1}{\rho_o} - \frac{1}{\rho}\right) \quad , \tag{26}$$

which is the Rankine-Hugoniot relation for conservation of energy across the shock, and solving for p as a function of $x = \rho_o/\rho$. In this relation, p and $\rho$ are the pressure and density immediately behind the shock; $I_o$ and $\rho_o$, the energy and pressure for the undisturbed state are taken equal to zero.

Before proceeding further with the explicit forms of the Hugoniot functions it is well to fix the notation to be followed. Since throughout the report only Hugoniot values of the flow variables will be used there is no need to distinguish values immediately behind the shock in either projectile or target from values well behind the shock. Thus no subscripts will be used to denote Hugoniot values except at the instant of impact when a subscript i

will appear. Barred letters will be used for the projectile medium, unbarred for the target medium and a subscript o will denote the undisturbed state before impact. Pressure, density, particle velocity, shock velocity and specific internal energy are represented by the letters p, $\rho$, u, $\dot{R}$ and I, respectively. $V_o$ denotes projectile velocity.

In obtaining the Hugoniot functions for the projectile material of subnormal bulk density, $\bar{\rho}_o < \rho_o$, it is convenient to introduce the "porosity ratio"

$$\delta = \bar{\rho}_o / \rho_o \tag{27}$$

and the density ratio

$$\bar{x} = \rho_o / \bar{\rho} .$$

The Hugoniot function for the projectile material, which we denote by $\bar{p}(\bar{x})$, can then be obtained by substituting

$$\bar{I} = \frac{\bar{p}}{2\bar{\rho}_o} (1 - \delta \bar{x}) \tag{28}$$

into $\bar{p} = f(\bar{\rho}, \bar{I})$ and solving for $\bar{p}$ as a function of $\bar{x}$. This procedure enables one to obtain an expression for the Hugoniot of a reduced density material from the equation of state for the same material of normal density. Experimental verification of data obtained using this procedure is documented in a series of recent Soviet publications (references 8, 9, 10). The relation (28) is the same as relation (26) but written for the projectile material. It insures the correct internal energy behind the shock propagating into the projectile material.

With these notations the Hugoniot function $\bar{p}(\bar{x})$ turns out to be

$$\bar{p} = 2\delta \left\{ \frac{F_2(\bar{x}) - \sqrt{F_2^2(\bar{x}) - F_1(\bar{x}) F_3(\bar{x})}}{F_1(\bar{x})} \right\}, \quad 0 < \bar{x} < 1/\delta \tag{29}$$

where

$$F_1(\bar{x}) = \bar{x}(1 - \delta\bar{x})\left[(1 - \delta\bar{x})\left|(c_o - c_1)\bar{x} + c_1\right| - 2\delta\bar{x}\right] ,$$

$$F_2(\bar{x}) = \delta\Phi_o\bar{x}^2 - \frac{1}{2}(1 - \delta\bar{x})\left|b_o\bar{x}^2 + (1 - \bar{x})\left[(b_1 - b_2)\bar{x} + b_2\right]\right| ,$$

$$F_3(\bar{x}) = (1 - \bar{x})\left[a_1\bar{x} + a_2\left|1 - \bar{x}\right|\right] .$$

Bars are not put above the material parameters $a_1$, $a_2$, etc. since the projectile and target materials are the same except for their equilibrium densities ($\bar{\rho}_o$ and $\rho_o$).

If we denote the right side of (29) by H ($\bar{x}$, $\delta$ ), then in terms of this functional notation the Hugoniot for the target material is written down directly as

$$p = H(x, 1) \quad , \; 0 < x < 1 \quad , \tag{30}$$

so that (29) becomes identical with the target material Hugoniot as $\delta \to 1$.

To compute the Hugoniot values of pressure, density, particle velocity and specific internal energy at the time of impact it is convenient to write down the relations (in laboratory coordinates) for the conservation of momentum, mass and energy across the shocks which begin propagating in the projectile and target materials at this time. Written down in parallel fashion for the two media we have:

| PROJECTILE | TARGET | |
|---|---|---|
| $\bar{p}_i = \bar{\rho}_o(V_o - u_i)(V_o + \dot{\bar{R}}_i)$ | $p_i = \rho_o u_i \dot{R}_i$ | (31) |
| $(1 - \delta\bar{x}_i)(V_o + \dot{\bar{R}}_i) = V_o - u_i$ | $(1 - x_i)\dot{R}_i = u_i$ | (32) |
| $\bar{I}_i = \frac{p_i}{2\bar{\rho}_c}(1 - \delta\bar{x}_i)$ | $I_i = \frac{p_i}{2\rho_o}(1 - x_i)$ | (33) |

Already incorporated into these equations is the fact that at impact pressure and particle velocity are continuous across the interface, i.e.

$$\bar{p}_i = p_i \quad , \qquad \bar{u}_i = u_i \quad .$$

Eliminating the initial shock velocities from (31) and (32) and observing (33) we obtain the relations

$$V_o - u_i = \sqrt{\frac{p_i(1 - \delta\bar{x}_i)}{\bar{\rho}_o}} = \sqrt{2\bar{I}_i} \; ; \; u_i = \sqrt{\frac{p_i(1 - x_i)}{\rho_o}} = \sqrt{2I_i} \quad .$$

By adding these relations and substituting $H(\bar{x}_i, \delta)$ for $p_i$ in the first of them and $H(x_i, 1)$ for $p_i$ in the second, we obtain

$$\sqrt{\frac{(1 - \delta\bar{x}_i)H(\bar{x}_i, \delta)}{\bar{\rho}_o}} + \sqrt{\frac{(1 - x_i)H(x_i, 1)}{\rho_o}} = V_o$$

However, since $\bar{p}_i = p_i$, we have the additional equation

$$H(\bar{x}_i, \delta) = H(x_i, 1)$$

The simultaneous solution of (35), (36) yields $x_i$ and $\bar{x}_i$ and their substitution into (34) then allows $u_i$, $I_i$, $\bar{I}_i$, $p_i$ to be evaluated. A simple iterative program for computing these Hugoniot values has been written and used on the IBM 1620. The results of these computations are displayed graphically in Figures 3 through 7.

Figures 3 and 4 show plots of the Hugoniot function (29) for normal density aluminum and for the reduced densities $\bar{\rho}_o$ = 0.9, 0.44, 0.2 and 0.1 gm/cc. Impact velocities corresponding to the pressures generated at impact of projectiles of these densities with normal density aluminum are indicated on the curves. A striking feature of the curves is their multi-valuedness for $\bar{x} > 1$. This multi-valuedness in effect reflects a property which is characteristic of a porous medium, namely that it has negligible resistance to even a very weak compressive force, being collapsed to normal density almost instantaneously. Hence for $\dot{V}_o \doteq 0$ one expects, with this model for the behavior of a porous medium, that the corresponding Hugoniot value is $\rho = \rho_o$, and thus the Hugoniot curves in Figures 3 and 4 will swing back to pass through the point $\bar{x}_i = \frac{\rho_o}{\bar{\rho}} = 1$.

Figure 5 which is a crossplot of Figures 3, 4 shows the initial impact pressures as functions of the impact velocity. For densities of 0.2 and less, it appears that there is an upper limit to the pressures achievable through

subjecting the material to very strong shocks. For $\bar{\rho}_o = 0.1$ this limiting pressure is approximately 1.65 Mb.

Figure 6 gives the variation with impact velocity of the density ratios $\rho/\rho_o$ and $\bar{\rho}/\rho_o$ in the target and projectile, respectively. In the target the density ratio $\rho/\rho_o$ increases monotonely as the impact velocity increases whereas in the projectile the corresponding density ratio $\bar{\rho}/\rho_o$ decreases to a minimum and then increases. For densities below 0.44 gm/cc this minimum occurs at approximately $V_o = 15$ km/sec. For subnormal densities of 0.2 and less, it is evident that extremely strong shocks will not compress the material to normal density. A reason for this is supplied by Figure 7 which shows how the specific internal energies I, $\bar{I}$ behind initial shock fronts in the target and projectile materials vary with increasing impact velocity. It will be noted that $\bar{I}$ increases rapidly with $V_o$ and particularly so for the smaller values of $\bar{\rho}_o$. At such elevated values of $\bar{I}$ and corresponding high temperatures the projectile density $\bar{\rho}$ is kept well below the normal density of $\rho_o = 2.702$ gm/cc.

## RESULTS AND DISCUSSION

1. The analytical model for computing peak axial pressures in thick targets impacted at hypervelocities by end-on oriented right circular cylindrical projectiles was extended to include subnormal density projectiles. The computer program (PICWICK I) calculations used to aid in making this extension were for impacts of subnormal density aluminum projectiles into normal aluminum at an impact speed of $V_o$ = 20 km/sec. (= 2 cm/$\mu$sec). Two such impact cases were run, one for a projectile density of 0.9 gm/cc and the other for 0.44 gm/cc, in each case the same size projectile being used, namely a cylinder of radius = length = 0.26192 cm. (Volume equivalent to a 3/16" diameter sphere).

The peak axial pressure in megabars obtained in the PICWICK calculations for the projectile density of 0.9 gm/cc is shown by the set of solid points plotted in Figure 8 as a function of the distance R (in cm) below the target surface. The encircled points give the corresponding times since impact (in $\mu$sec). The analytical model furnishes the corresponding continuous pressure and time profiles, the dotted portions corresponding to the region of high unattenuated impact pressure up to the time when lateral rarefaction fronts finally relax the peak pressure on the axis of penetration. This pressure stays at approximately 2.55 Mb over a distance of 0.305 cm and a time of 0.25 $\mu$sec. For a solid aluminum projectile of normal density with the same size and speed the impact pressure is 4.88 Mb (see Figure 3), a much higher value owing to the larger impacting energy. Figure 8 indicates a rapid decline in peak pressure, the pressure pulse being effectively dissipated within the first two centimeters of target material. The time versus axial distance of the shock front advancing into the target is replotted in Figure 9 on log-log paper. This plot indicates that the analytic solution exhibits shortly after impact a linear variation in the variables log R, log t, implying thereby an R, t-relation of the form $R \backsim t^{2/3}$. In general, one would expect for the log R, log t-plot a profile curve of the type shown in Figure 10: initially, over the unattenuated pressure region, $R = \dot{R}_i t$, giving rise to the initial straight portion of the profile with slope = 1, the next portion covers the shock speed range $\dot{R}_i > \dot{R} > c_o$ between the impact shock speed $\dot{R}_i$ and the undisturbed sound speed $c_o$, in which portion the 2/3 slope is attained for a certain time interval; as the shock decays into an elastic wave one has the variation $R = c_o t$, giving rise again to a segment of slope = 1. The 2/3 is of interest in comparison with that predicted by other analytical models for hypervelocity impact. One such model (ref. 7) assumes a point source of instantaneous energy release giving rise to a spherical blast wave with self-similar flow behind the front. For such a model the R, t relation assumes the form $R \backsim t^{0.4}$. For comparison the 0.4 slope is indicated in Figure 9. As is evident the (R, t) points from the PICWICK I computer program calculations show a distinctly different trend, being reasonably close to the analytic solution proposed in this report.

Computer program computations for the 20 km/sec impact of the 0.44 gm/cc projectile appear in Figure 11 along with the continuous profiles obtained through use of the analytical model. The R, t-plot on log-log paper is shown in Figure 12. The same characteristics observed in Figures 8, 9 apply also to Figures 11, 12, namely the initial region of unattenuated pressure followed by a rapid decline; the shock penetration versus time variation of the form $R \backsim t^{2/3}$ during the major portion of this decline; and the fairly good agreement of the model with the computer results. The impact pressure is 1.74 Mb, reflecting the smaller projectile energy associated with the lower density. The pressure pulse is effectively dissipated over the first 1.5 cm of target material.

2. A principal aim of the present report is the use of a specific analytical model for investigating the effect of a projectile's density on the pressure pulse which propagates into the target. An initial investigation of the effect was reported in reference (4) where computations were made using the PICWICK I computer program comparing the flow fields generated by equi-mass cylindrical projectiles of aluminum of densities 2.702, 0.9 and 0.44 gm/cc impacting a thick normal density aluminum target. In each case the radius L of the projectile was taken equal to its length $\ell$ and the impact velocity was kept at 20 km/sec. For the normal density projectile L was taken to be 0.26192 cm. In keeping with the equi-mass assumption, the reduced density projectiles were accordingly larger, the radii of the 0.9 gm/cc and 0.44 gm/cc projectiles being, respectively, 0.37782 and 0.47965 cm. For comparison of the flow fields generated by these three projectile impacts calculations were made of the total momenta of the flows both in the forward axial direction and in the outward radial direction. These are shown plotted in Figures 13 and 14. The agreement for each of the momentum plots is quite remarkable. In addition to these plots the magnitude of the peak axial pressure as a function of the distance below the target surface was plotted for each of these impacts in Figure 15. The pressure values from the PICWICK program are of course much rougher than the integrated total momenta; nevertheless, approximate coalescence of these profiles is evident well above 0.3 Mb which is the estimated threshold pressure in aluminum below which strain-rate and strength effects become important during the cratering process (see ref. 4). This fact, together with the agreement in the total momentum plots of the three impact situations, leads to the conclusion that the density of the projectile has no essential effect at least for the case of aluminum with density as low as 0.44 gm/cc.

3. Since, as discussed in the INTRODUCTION, interest centers about the impact effect of particles of average bulk density as low as 0.2 gm/cc, a logical first step would be to extend the computer program (PICWICK) calculations to projectile densities below 0.44 gm/cc and also for impact velocities down to the lower limit of interest, namely 7.6 km/sec. This is presently being done; but, owing to the finer resolution required in the calculations, the continuous

mass code (PICWICK III) will have to be used. At this time results for the lower densities and velocities are not yet available.

A preliminary investigation in this direction can, however, be made using the analytical model to compare peak axial pressure profiles for equi-mass impacts at a given velocity as described above. The results of such an investigation are presented in Figures 16 and 17. The subnormal densities used, in addition to the 0.9 and 0.44 gm/cc cases, were 0.2 gm/cc and 0.1 gm/cc. Equi-mass cylindrical projectiles (L = $\ell$) of the latter two densities have radii L = 0.6238 cm and L = 0.7859, respectively. For completeness we list below the densities and sizes of the five impacting projectiles considered in Figures 16, 17.

| $\bar{\rho}_o$ (gm/cc) | L (cm) | $\delta = \bar{\rho}_o/\rho_o$ |
|---|---|---|
| 2.702 | 0.2619 | 1.0 |
| 0.9 | 0.3778 | 0.333 |
| 0.44 | 0.4797 | 0.163 |
| 0.2 | 0.6238 | 0.074 |
| 0.1 | 0.7859 | 0.037 |

The impacts in Figure 16 are for $V_o$ = 20 km/sec, those in Figure 17 for $V_o$ = 7.6 km/sec.

The peak axial pressures are plotted in Figure 16 as a function of distance penetrated below the target surface. Their early coalescence for the densities 2.702, 0.9, 0.44 verifies the computer program (PICWICK I) results shown in Figure 15, thereby lending some measure of confidence in the profiles displayed for the 0.2 and 0.1 density cases. Indeed, this coalescence for $\bar{\rho}_o \geq 0.44$ is quite remarkable. Thus, for projectile densities above 0.44 gm/cc it appears quite conclusive that a thick aluminum target experiences the same peak axial pressures for different equi-mass impacts of a given hypervelocity beyond only a short initial distance into the target.

Times of arrival of the peak of the pressure pulse at given axial locations are also plotted for the five impacts in Figure 16. For the projectile densities 2.702, 0.9, and 0.44 gm/cc, the corresponding time profiles tend to differ by a constant amount. Thus the curve for the 0.9 impact is approximately .07$\mu$ sec higher than that for the 2.702 impact and that for the 0.44 impact is about .15$\mu$ sec higher. The same result was observed in the computer program (PICWICK I) calculations in reference 5 where the values .05 and .12 $\mu$sec were estimated by smoothing rather rough data. This furnishes another measure of confidence in the analytical model in relation to the computer program results. The time curves for the 0.2 and

0.1 density cases do not show common "parallelism" with the other time curves, as might be expected judging from the non-coalescence of the pressure profiles.

Figure 17 shows the results of the equi-mass impacts at the lower limit of the velocities of interest, 7.6 km/sec. Here, as in Figure 16, the pressure profiles for the 0.2 and 0.1 cases are clearly distinct from the profiles for the higher densities. There is coalescence of the profiles for the 0.9 and 0.44 density impact cases at about 0.2 Mb, which is already within the 0.3 Mb threshold for strain-rate and strength effects. Their additional coalescence with the profile for the 2.702 impact is approximate only, occurring at very low pressure. Since the analytical model does not incorporate strain-rate and strength effects into its formulation, being entirely a hydrodynamic model, about all one can conclude here is that the lower limit of subnormal projectile density to give "density effect independence" in impacts is above 0.9 gm/cc. However, the strong departure of the pressure profiles in the 0.2 and 0.1 gm/cc cases from those corresponding to the higher density cases does suggest, as in the 20 km/sec impacts, a higher level of peak pressure propagating in the target for very low density projectiles of a given mass and impact velocity. The time profiles of peak pressure arrival at axial locations R are also presented in Figure 17. The curves corresponding to the 0.9 and 0.44 gm/cc densities show a constant separation of 0.18 $\mu$sec and an approximate separation from the $\bar{\rho}_o$ = 2.702 time profile of 0.225 and 0.405 $\mu$sec, respectively.

It is apparent from Figures 16 and 17 that the pressure profiles for the impact cases involving the low projectile densities of 0.2 gm/cc and 0.1 gm/cc are separate and distinct from those corresponding to projectile densities of 0.44 and above. This is quite unexpected and contrary to intuition. Since the analytical model used to compute these profiles is strongly dependent on the form of the Hugoniot function employed for the subnormal density projectile material, it is not possible to say at this time whether this phenomenon represents physical fact or is a consequence of the specific model adopted for the behavior of the reduced density material under compression. To help settle this question one would need to make a sensitivity study of the analytical model in which variations of the pressure profiles with changes in its basic inputs would be considered.

## CONCLUSIONS

1. It has been shown that an existing analytical model which describes peak axial pressures in a thick target impacted at hypervelocity by a cylindrical projectile of like material can be extended to describe impacts by projectiles of like material but of subnormal bulk density. The peak pressures and their times of arrival at axial locations in the target are in good agreement with the results obtained from a numerical solution of the defining partial differential equations through the use of the PICWICK I hydrodynamic computer program for densities down to 0.44 gm/cc.

2. Subnormal bulk density projectiles of aluminum of a given mass impacting a thick normal density aluminum target at 20 km/sec show no special density effect on the peak pressures propagating into the target for projectile densities of 0.44 gm/cc and greater. At 7.6 km/sec the lower limit of projectile density for "density effect independence" is above 0.9 gm/cc.

3. For the very low subnormal bulk densities of 0.2 and 0.1 gm/cc the corresponding projectile impacts, on the basis of the specific model adopted here for the behavior of reduced density material under compression, yield peak axial pressure profiles which are separate and distinct from those obtained from impacts of equi-mass projectiles of higher density.

4. The analytical model presented here is strongly dependent on the form of the Hugoniot function employed for the subnormal density projectile material. Its sensitivity to other forms of the Hugoniot function needs to be evaluated before firm conclusions can be reached regarding the pressure profiles in the target arising from impacts by very low density projectiles.

# APPENDIX A

## SYMBOLS

| | |
|---|---|
| A | constant in shock propagation velocity eq. (7) |
| $a_1$, $a_2$ | constants in equation of state formula (25) |
| $b_o$, $b_1$, $b_2$ | constants in equation of state formula (25) |
| $c_o$, $c_1$ | constants in equation of state formula (25) |
| B | constant in eq. (5) |
| c | hydrodynamic sound velocity |
| D | constant in eq. (5) |
| E | specific projectile energy |
| F | Hugoniot function |
| f | equation of state function |
| $F_1$, $F_2$, $F_3$ | auxiliary functions used in defining Hugoniot F |
| H | Hugoniot function |
| h | function defining extrapolation of f along tangent line |
| I | specific internal energy |
| K | $k/\sqrt{I}$ |
| k | D/B |
| L | projectile radius |
| $\ell$ | projectile length |
| $\bar{L}$ | $\sqrt[3]{L^2 \ell}$ |
| p | Hugoniot pressure |
| R | axial coordinate |

| | |
|---|---|
| $R_1$ | point of convergence of lateral rarefaction fronts |
| $R_o$ | constant in eq. (7) |
| $t$ | time since impact |
| $t_i$ | time for lateral rarefaction to propagate to axis |
| $t_1$ | time associated with point $R_1$ |
| $u$ | particle velocity |
| $v_o$ | impact velocity |
| $x$ | $\rho_o/\rho$ |
| $\bar{x}$ | $\rho_o/\bar{\rho}$ |
| $\alpha$ | constant in formula for K |
| $\beta$ | constant used in evaluating A |
| $\delta$ | $\bar{\rho}_o/\rho_o$ |
| $\zeta$ | $\rho/\rho_o - 1$ |
| $\theta$ | off-axis angle |
| $\rho$ | density behind shock propagating into target |
| $\rho_o$ | undisturbed target density |
| $\bar{\rho}_o$ | undisturbed projectile density |
| $\Phi$ | $\rho_o I$ |
| $\Phi_o$ | constant in equation of state formula (25) |

Subscripts

| | |
|---|---|
| o | undisturbed state |
| i | value at impact (does not apply to letter t) |
| P | pertaining to projectile |
| T | pertaining to target |
| $\dot{R}$ | $dR/dt$ |

Bar above letter denotes corresponding quantity for the projectile material.

## APPENDIX B

## EQUATION OF STATE CONSTANTS FOR ALUMINUM

(gm-cm-$\mu$sec) - system of units

$$a_1 = 1.1867$$
$$a_2 = 0.76300$$
$$b_o = 3.4448$$
$$b_1 = 1.5451$$
$$b_2 = 0.96430$$
$$c_o = 0.43382$$
$$c_1 = 0.54873$$
$$\Phi_o = 1.5$$
$$\rho_o = 2.702$$

Note: In the gm-cm-$\mu$sec system the unit of pressure is the megabar.

(It is useful to remember that 1 km/sec = 0.1 cm/$\mu$sec.)

## REFERENCES


1. Clough, N. and Lieblein, S.: Significance of Photographic Meteor Data in the Design of Meteoroid Protection for Large Space Vehicles. NASA TN D-2958, 1965.

2. Lieblein, S., Clough, N., and McMillan, A. R.: Hypervelocity Impact Damage Characteristics in Armored Space Radiator Tubes. NASA TN D-2472, 1964.

3. Riney, T. D.: Solution of Viscoplastic Equations for Axi-symmetric Hypervelocity Impact, Summary Report APGC-TDR-62-74, November 3, 1961 - November 2, 1962.

4. Riney, T. D., and Heyda, J. F.: Hypervelocity Impact Calculations. Proc. Seventh Symposium on Hypervelocity Impact, Nov. 1964.

5. Heyda, J. F., and Riney, T. D.: Peak Axial Pressures in Semi-Infinite Media under Hypervelocity Impact. Proc. Seventh Symposium on Hypervelocity Impact, Nov. 1964.

6. Osborne, R. K. and his associates in Group W-4 at the Los Alamos Scientific Laboratory fitted the function f ($\rho$, I) to the equation of state data.

7. Davids, N., and Huang, S. W.: Shock Wave Propagation in Crater Formation. Journal of the Aerospace Sciences, Vol. 29, 1962, pp. 550-557.

8. Krupnikov, K., et al.: Shock Compression of Porous Tungsten, JETP 15, 470-476, (1962).

9. Kormer, S., et al.: Dynamic Compression of Porous Metals, JETP 15, 477-488 (1962).

10. Altshuler, L., et al.: Dynamic Compressibility and Equations of State of Iron under High Pressure, JETP 34, 606-614 (1958).

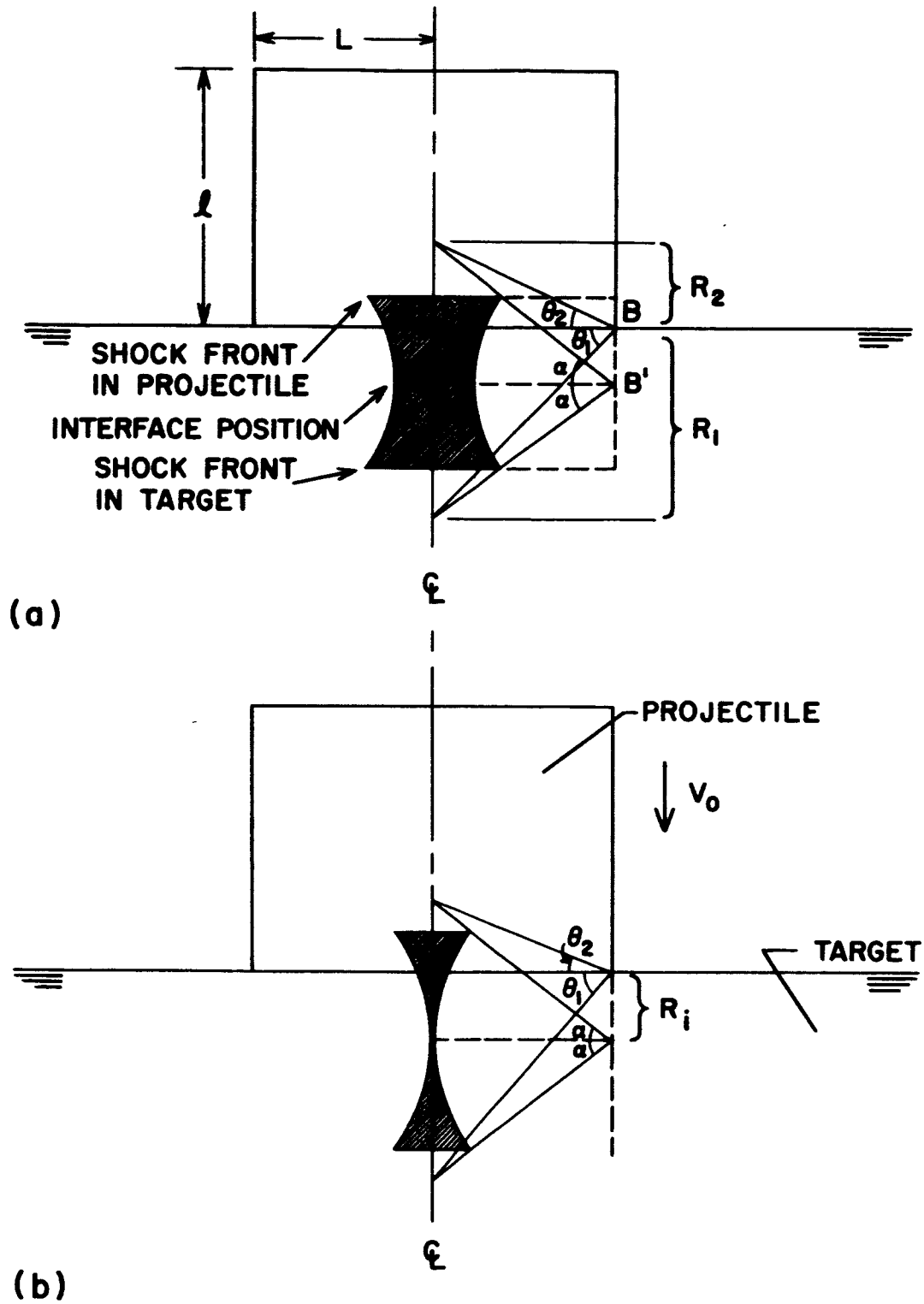


Figure 1. Sketch showing the central volume within which the material is still subjected to the unrelaxed peak shock conditions. The times depicted are (a) $0 < t < t_i$ and (b) $t = t_i$.

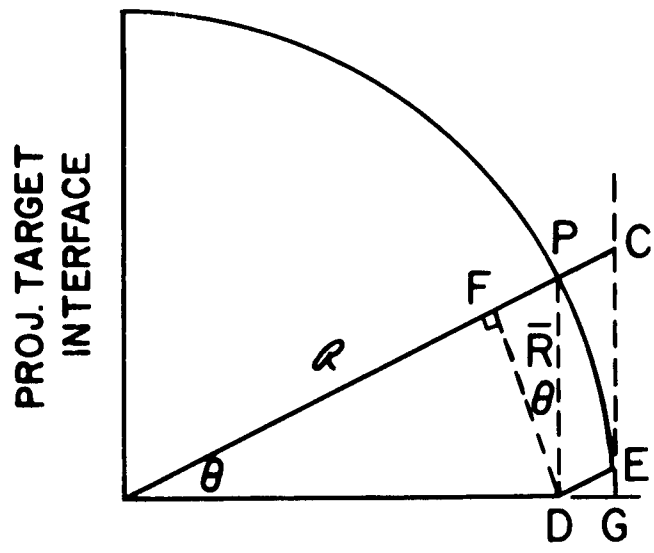


Figure 2. Shock geometry for derivation of speed of peak pressure pulse along axis of penetration.

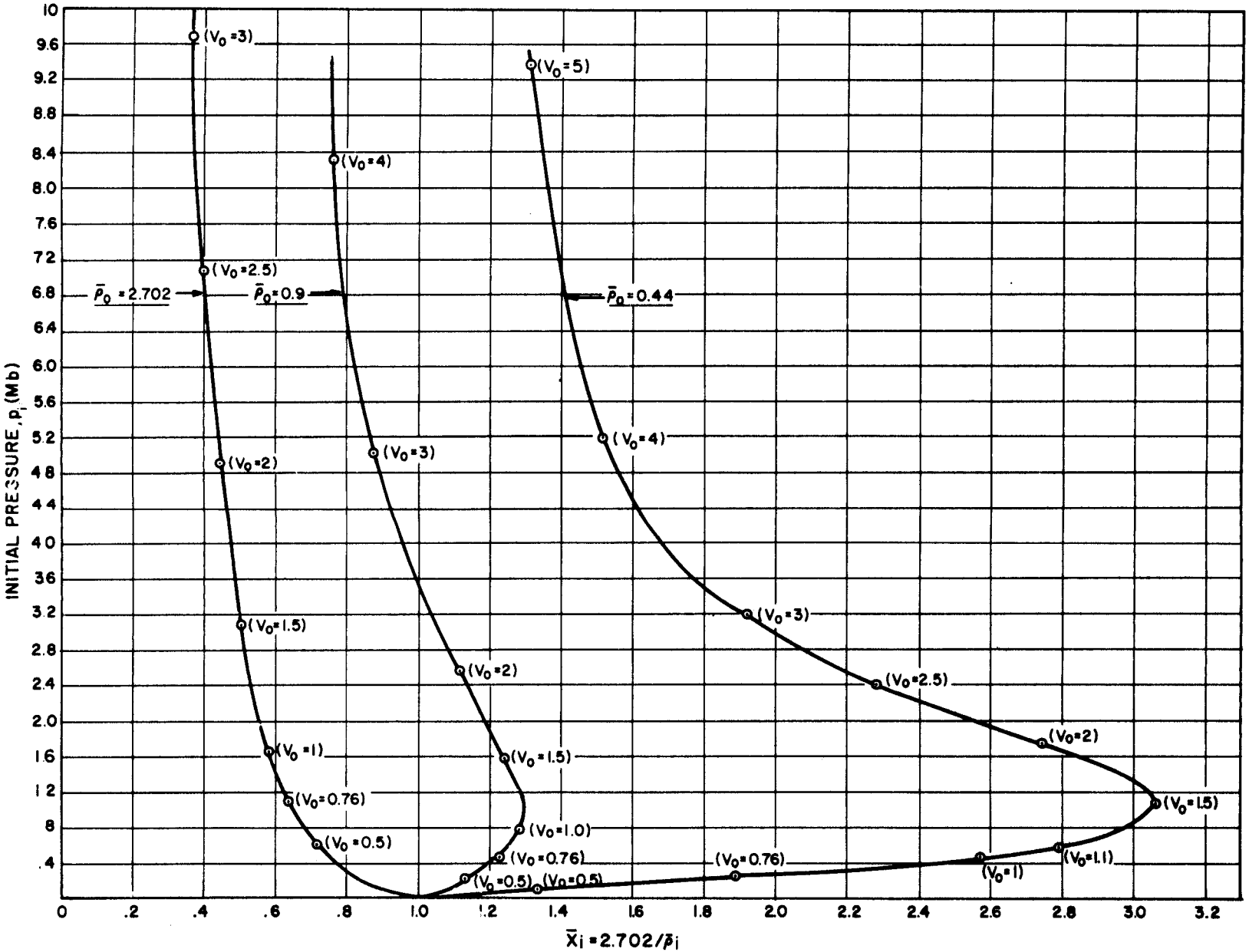


Figure 3. Hugoniot functions for normal density aluminum and for aluminum of subnormal bulk densities 0.9 gm/cc and 0.44 gm/cc.
($V_0$ in cm/$\mu$sec)

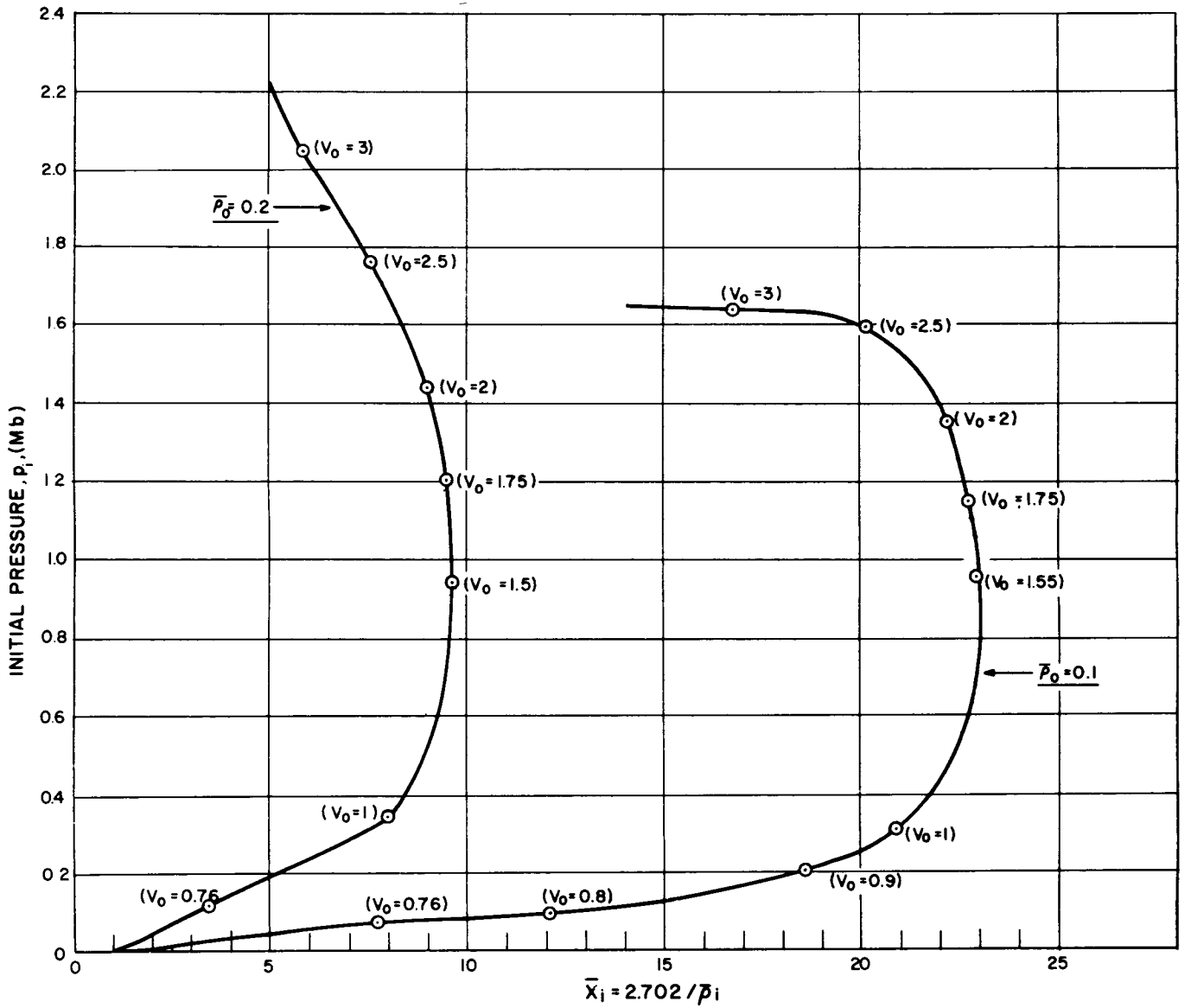


Figure 4. Hugoniot functions for aluminum of subnormal bulk densities of 0.2 gm/cc and 0.1 gm/cc. ($V_o$ in cm/$\mu$sec)

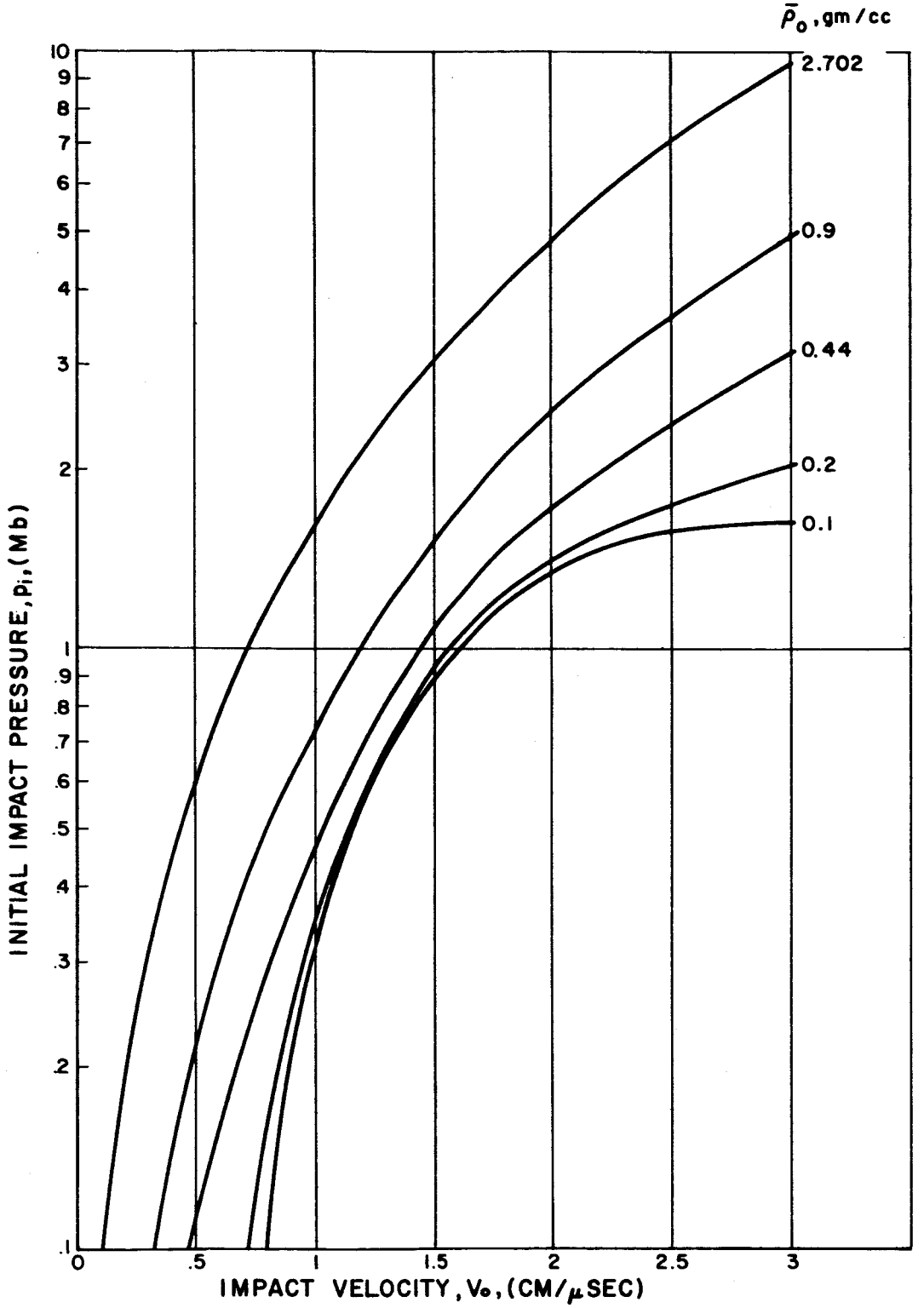


Figure 5. Initial impact pressures as functions of projectile impact velocity for normal and subnormal bulk density aluminum projectiles into aluminum target.

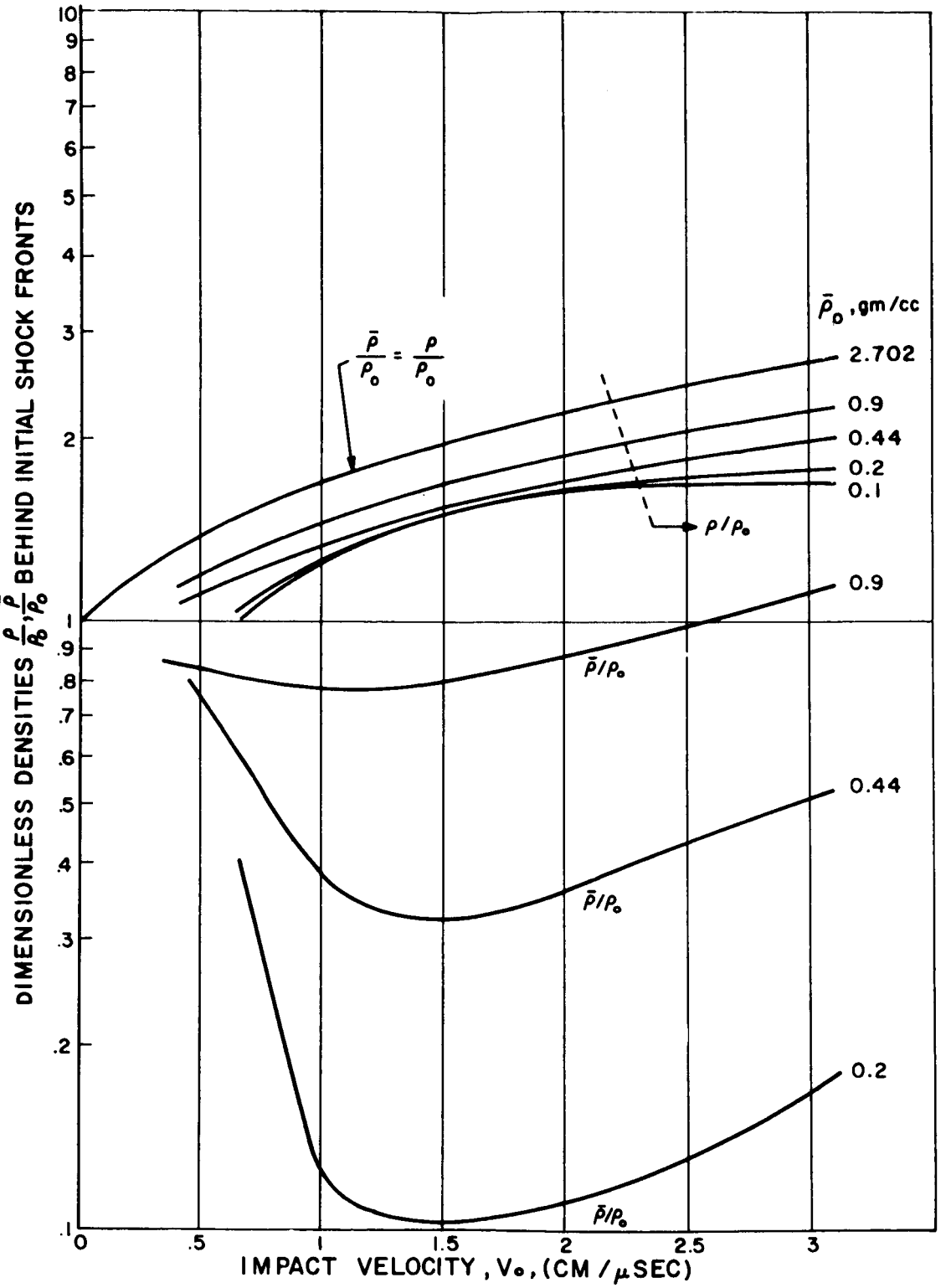


Figure 6. Dimensionless densities behind initial shock fronts in aluminum target and projectile as functions of projectile impact velocity.

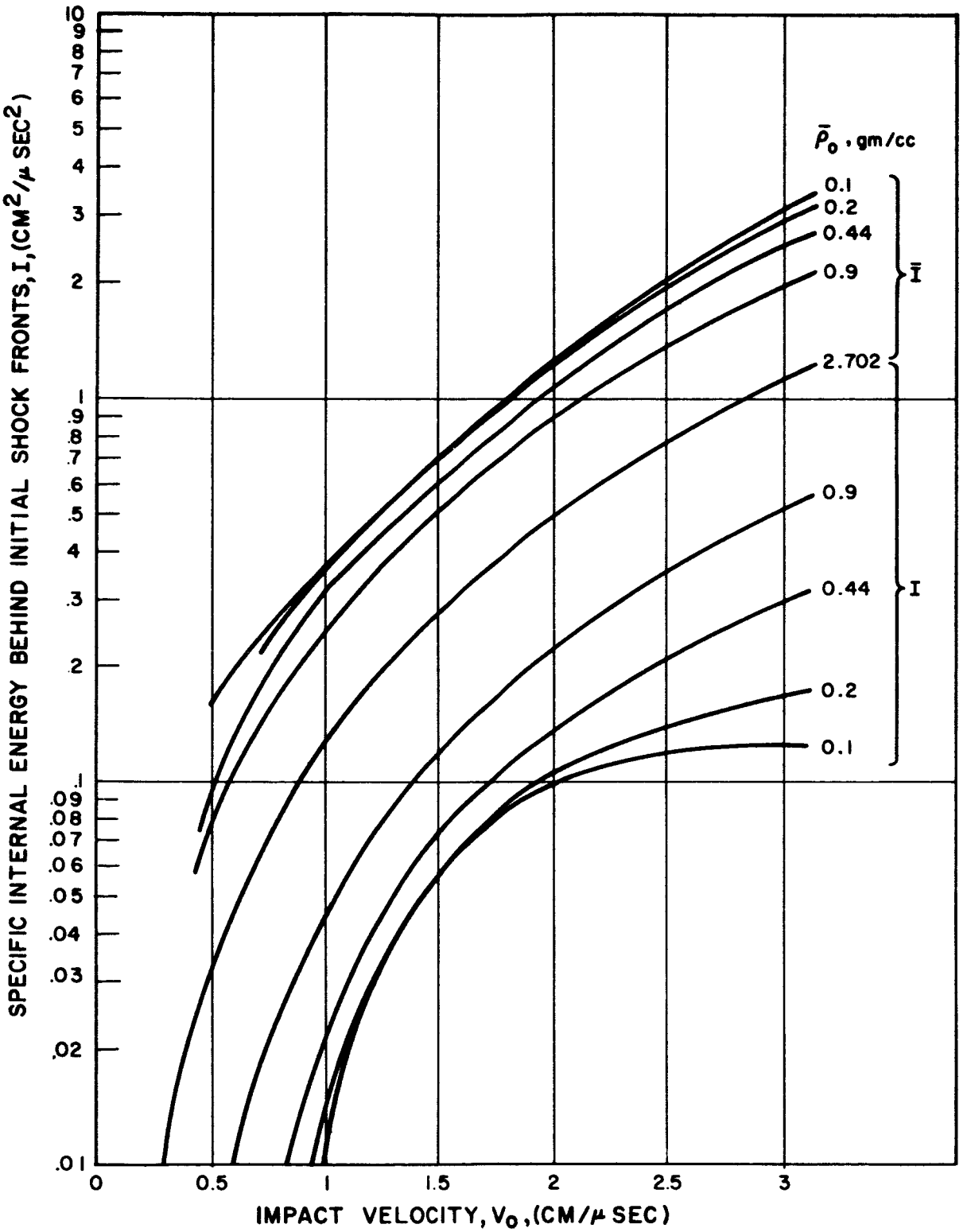


Figure 7. Variation of specific internal energy behind initial shock fronts in target and projectile with projectile impact velocity for normal and subnormal bulk density aluminum projectiles into aluminum target.

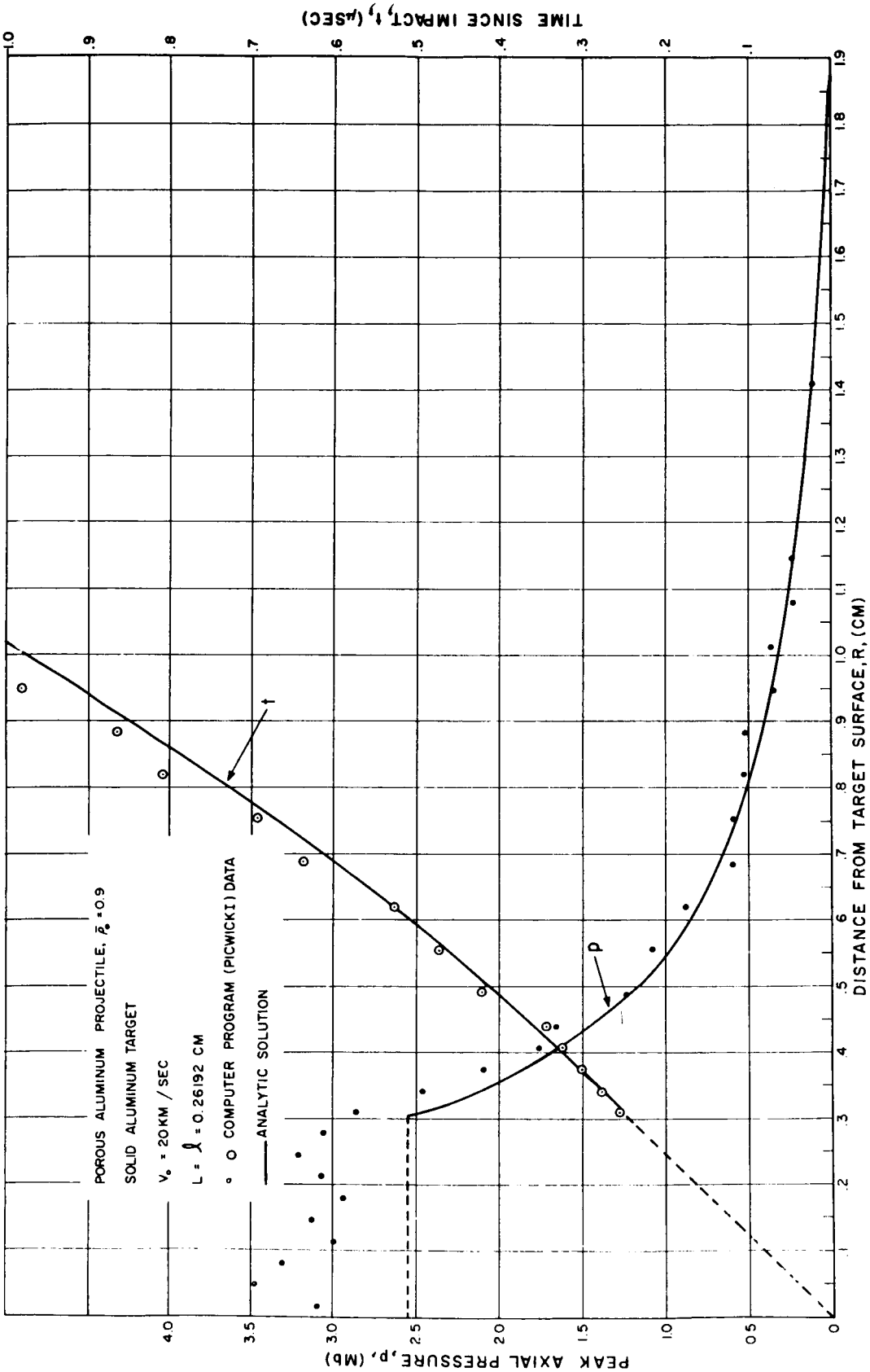


Figure 8. Peak axial pressure and time of arrival at axial location R.

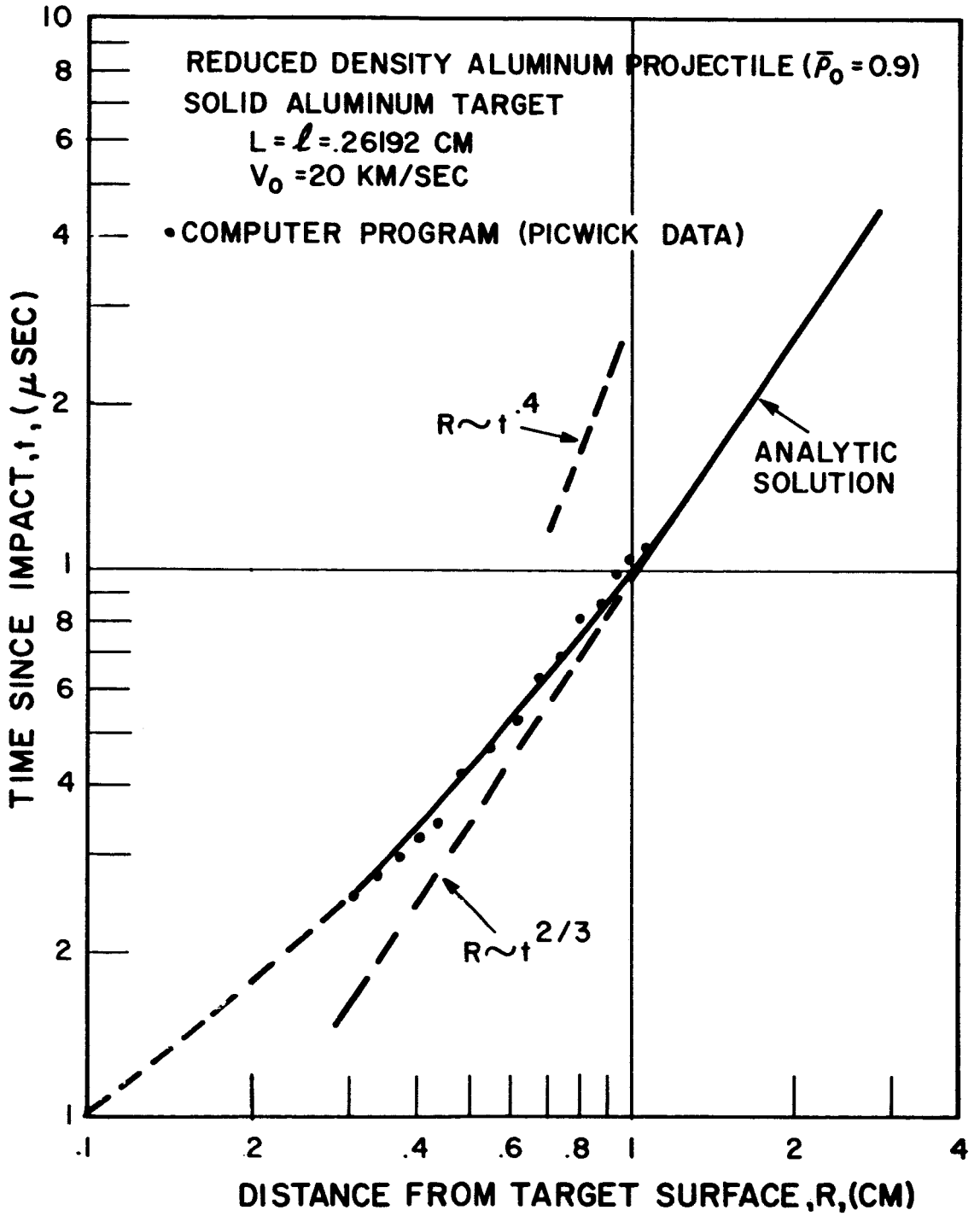


Figure 9. Log-log plot of shock penetration distance versus time since impact.

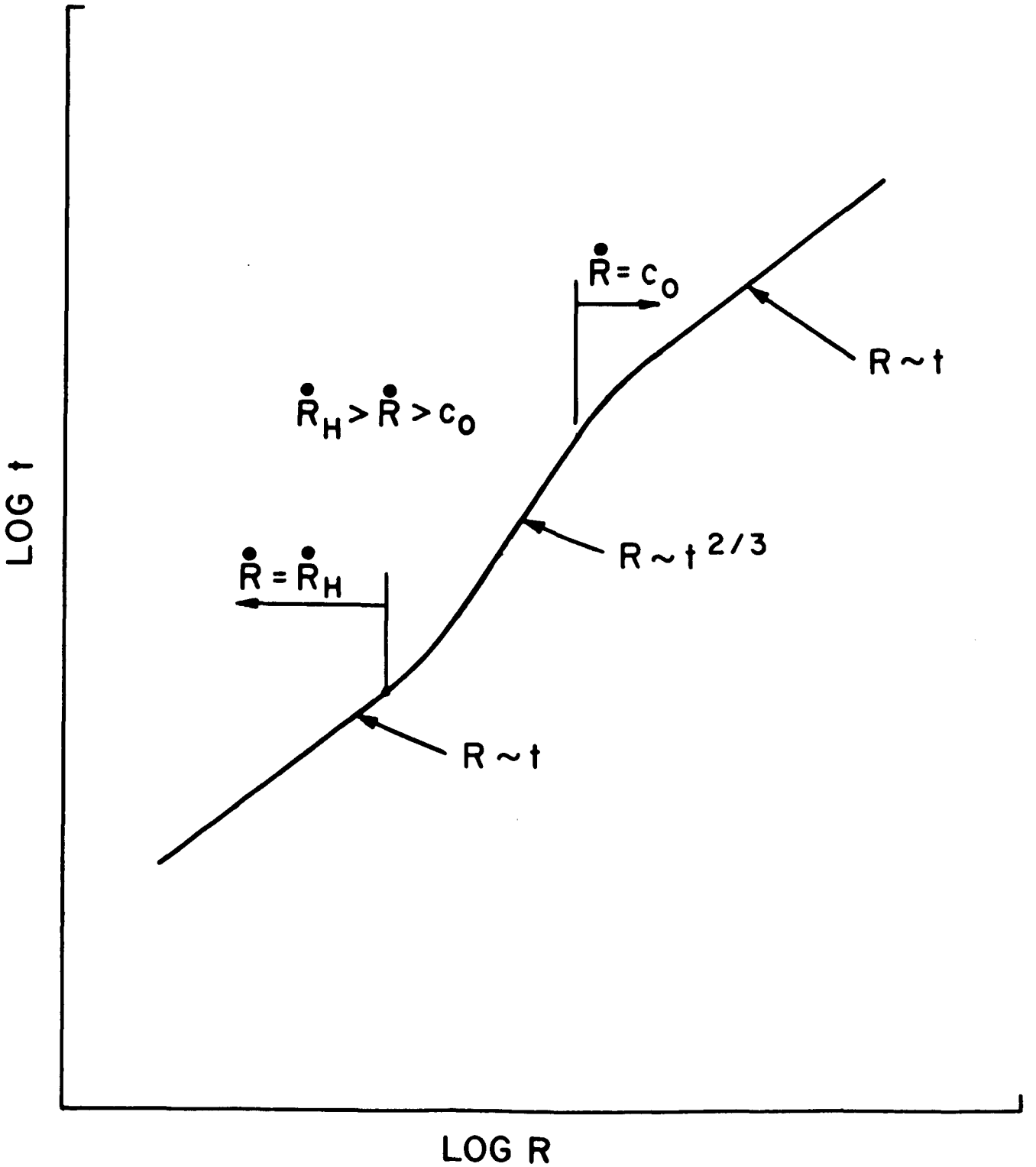


Figure 10. Schematic of shock penetration profile.

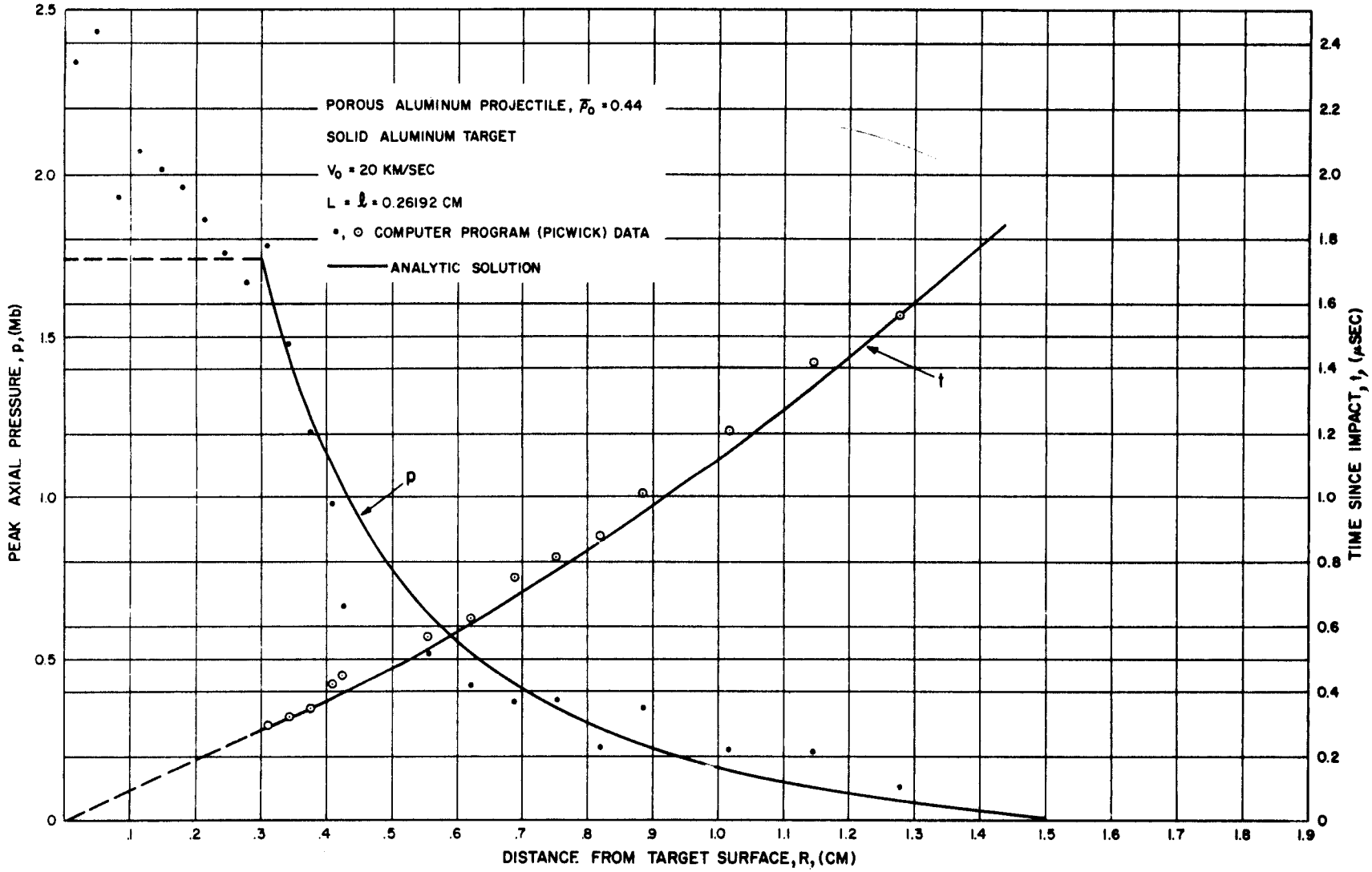


Figure 11. Peak axial pressure and time of arrival at axial location R.

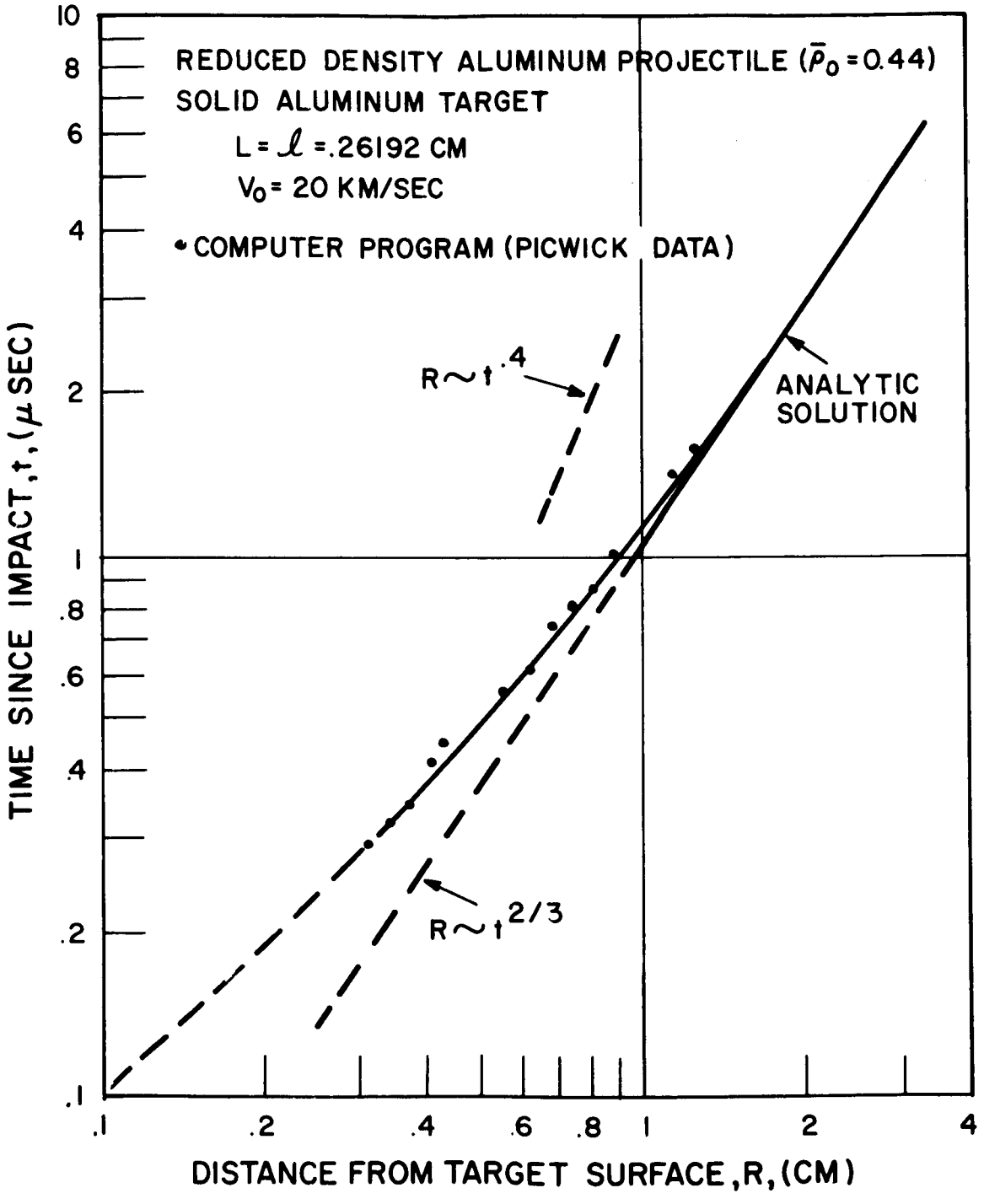


Figure 12. Log-log plot of shock penetration distance versus time since impact.

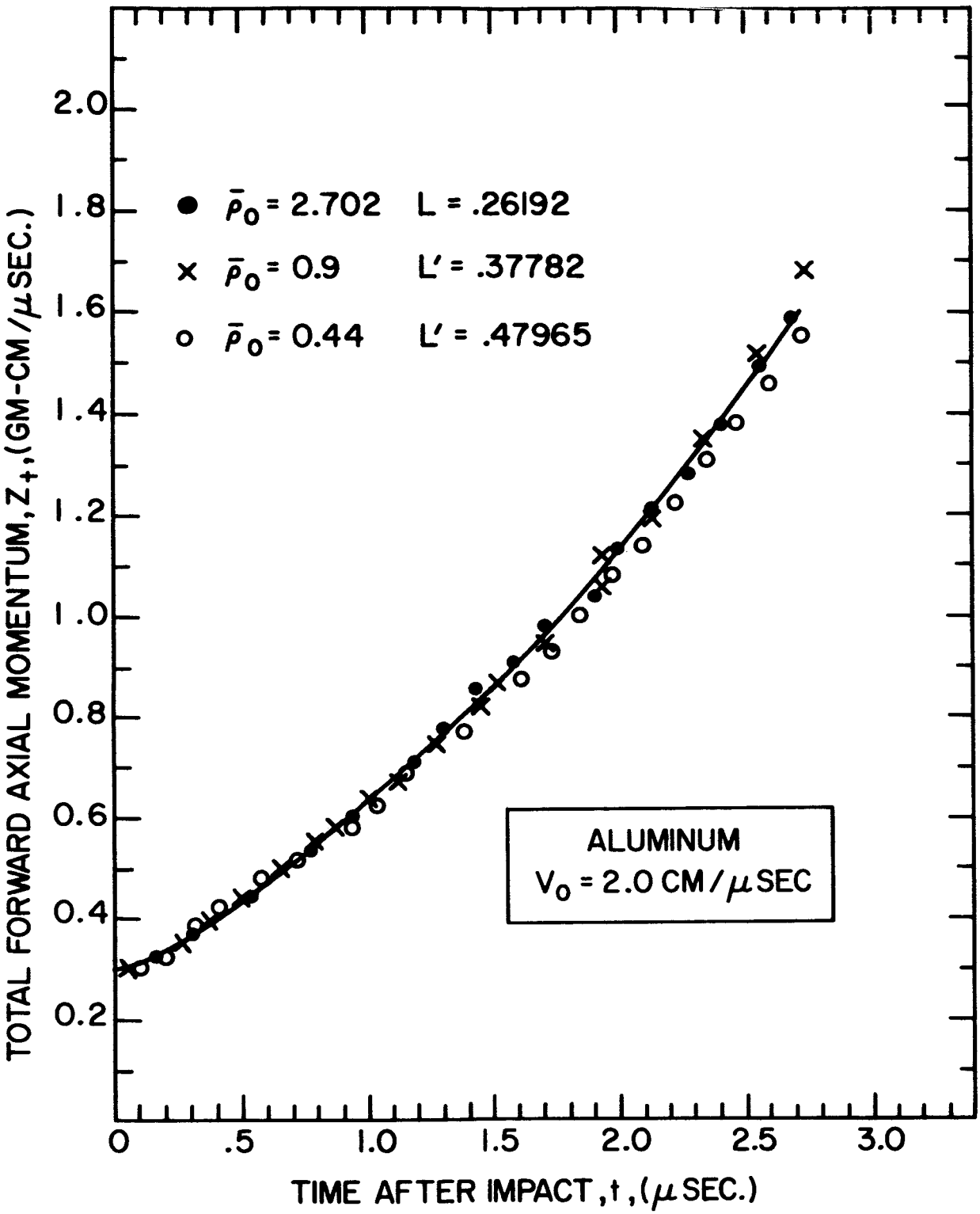


Figure 13. Total forward axial momentum for flow fields generated by equi-mass, equi-velocity aluminum projectiles of indicated bulk densities impacting an aluminum target at 2 cm/$\mu$sec. for time t after impact.

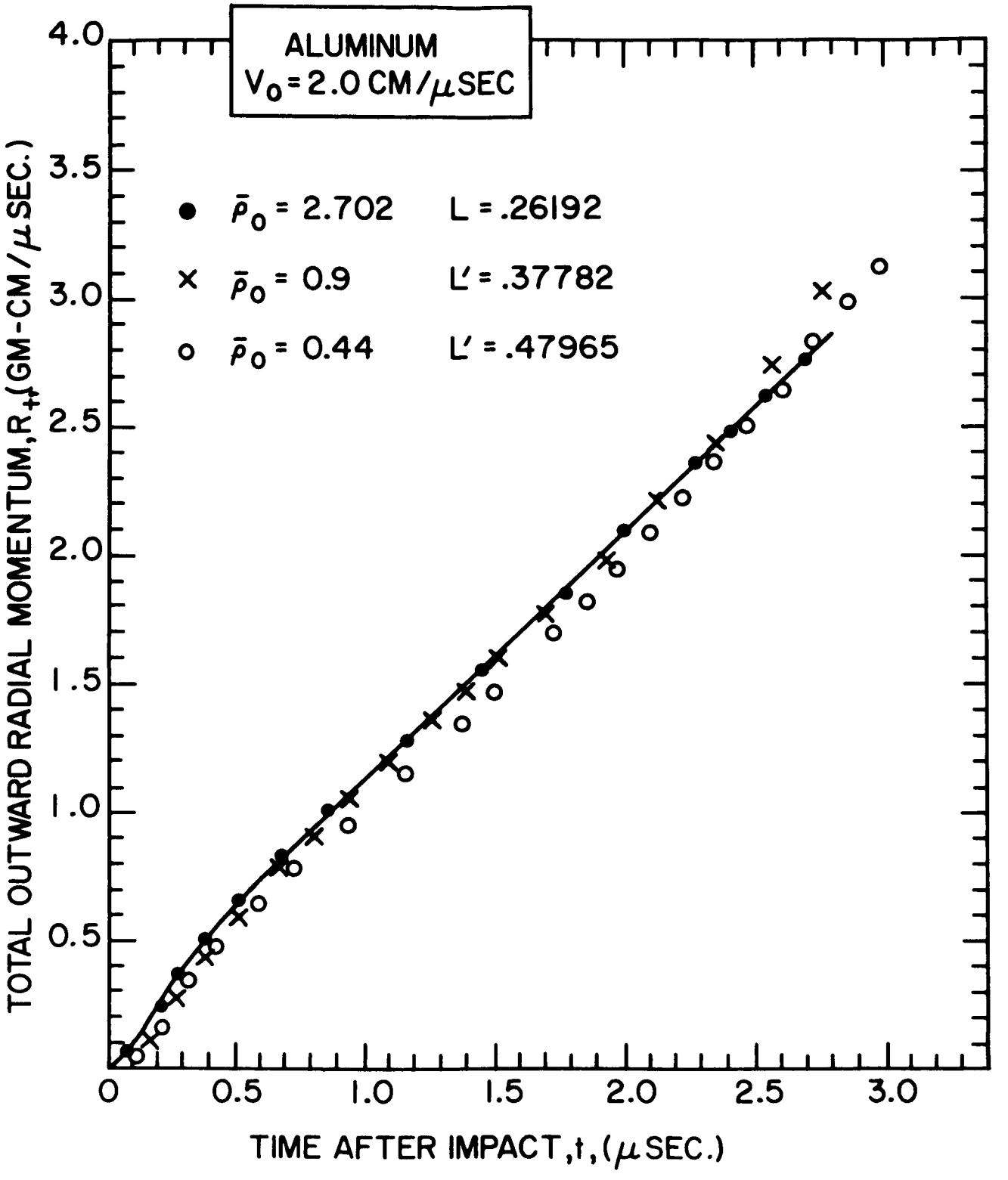


Figure 14. Total outward radial momentum for flow fields generated by equi-mass, equi-velocity aluminum projectiles of indicated bulk densities impacting an aluminum target at 2 cm/μsec. for time t after impact.

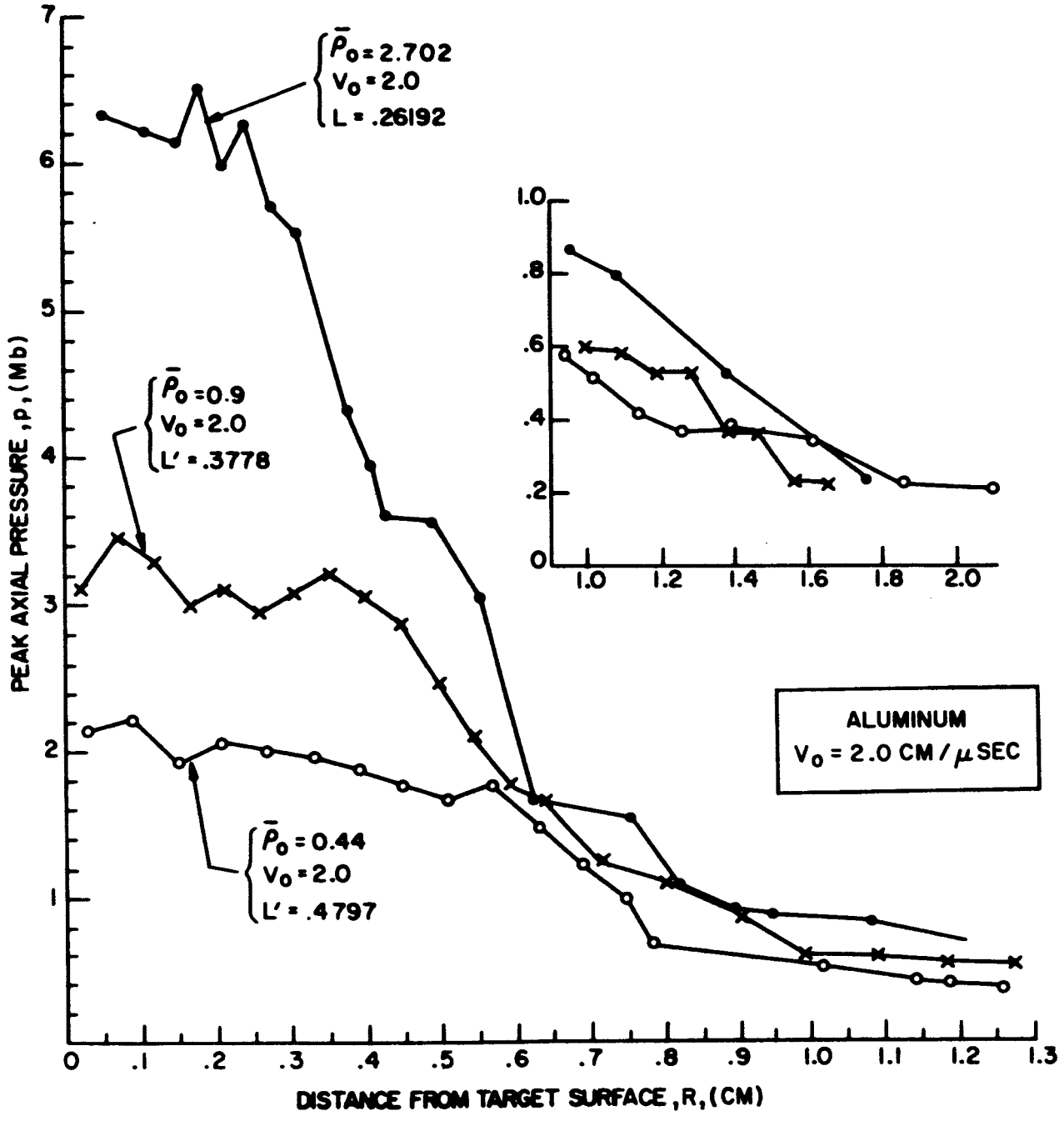


Figure 15. PICWICK I computations of peak axial pressures in aluminum target for impacts at 2 cm/$\mu$ sec of equi-mass aluminum projectiles of densities 2.702, 0.9 and 0.44 gm/cc. as functions of axial distance below target surface.

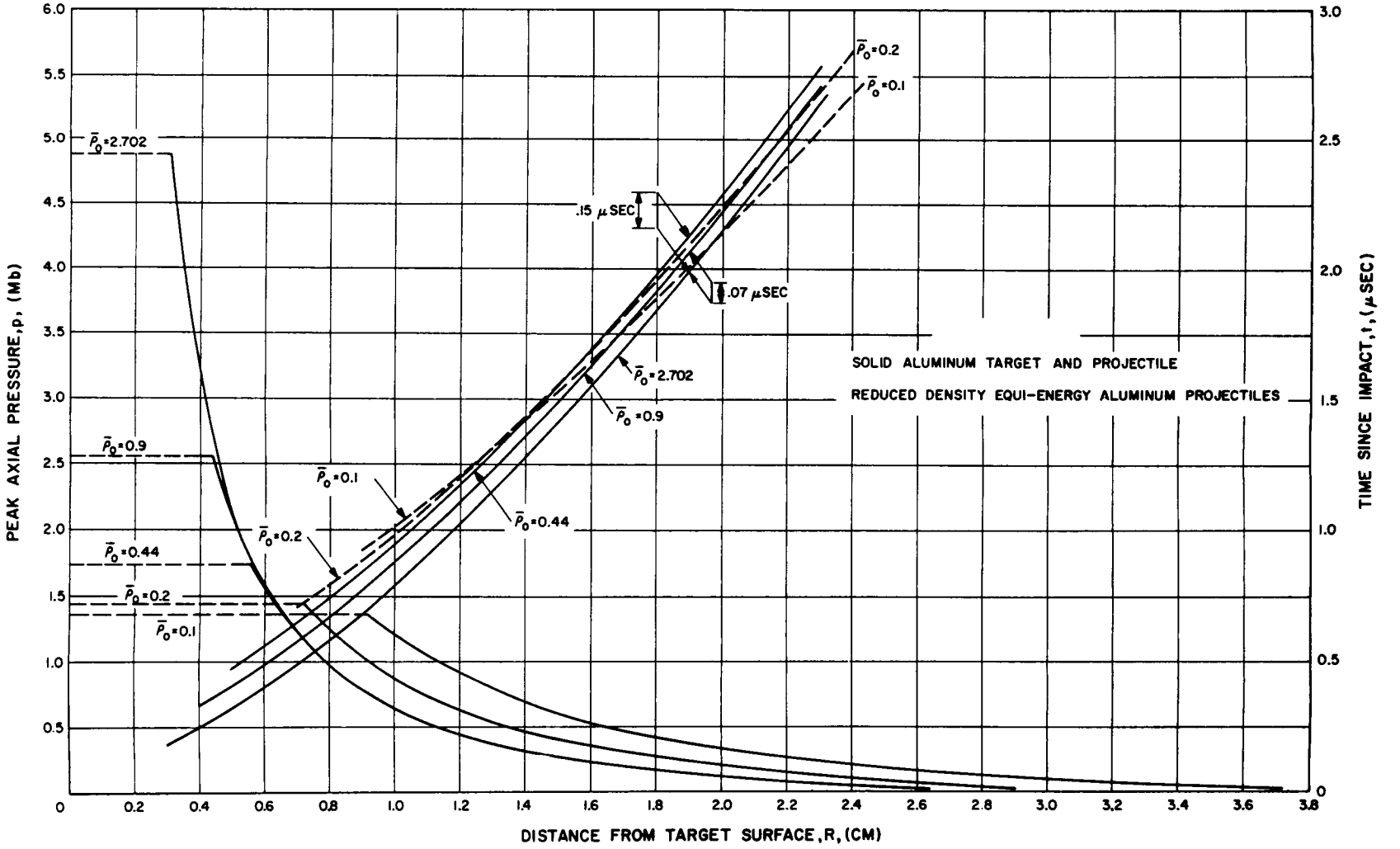


Figure 16. Peak axial pressures and times of arrival at axial locations R for equi-mass, equi-velocity projectiles. ($V_o$ = 20 km/sec)

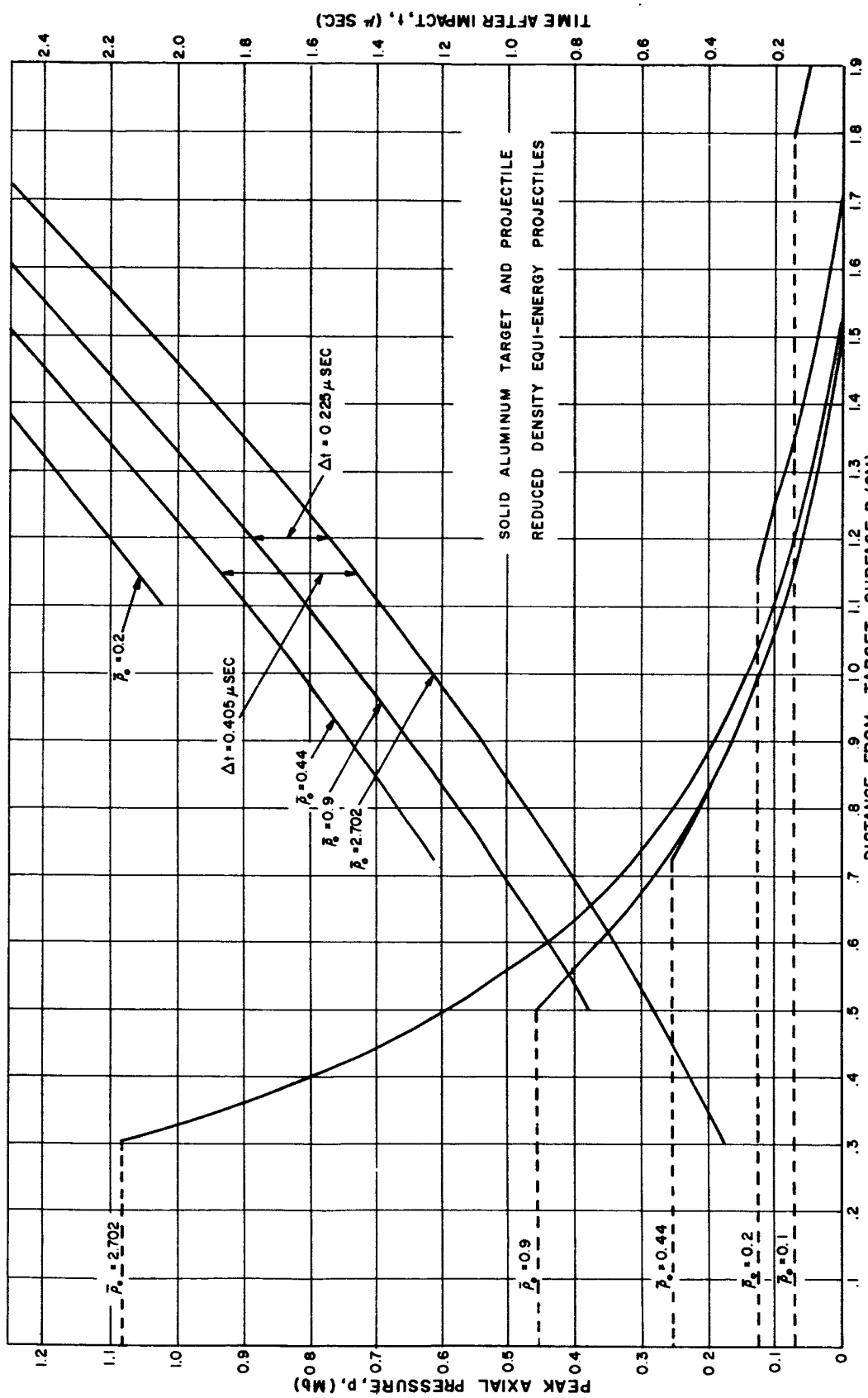


Figure 17. Peak axial pressures and times of arrival at axial locations R for equi-mass, equi-velocity projectiles. ($V_o$ = 7.6 km/sec)



NASA-Langley, 1966

*"The aeronautical and space activities of the United States shall be conducted so as to contribute . . . to the expansion of human knowledge of phenomena in the atmosphere and space. The Administration shall provide for the widest practicable and appropriate dissemination of information concerning its activities and the results thereof."*

—NATIONAL AERONAUTICS AND SPACE ACT OF 1958

# NASA SCIENTIFIC AND TECHNICAL PUBLICATIONS

**TECHNICAL REPORTS:** Scientific and technical information considered important, complete, and a lasting contribution to existing knowledge.

**TECHNICAL NOTES:** Information less broad in scope but nevertheless of importance as a contribution to existing knowledge.

**TECHNICAL MEMORANDUMS:** Information receiving limited distribution because of preliminary data, security classification, or other reasons.

**CONTRACTOR REPORTS:** Technical information generated in connection with a NASA contract or grant and released under NASA auspices.

**TECHNICAL TRANSLATIONS:** Information published in a foreign language considered to merit NASA distribution in English.

**TECHNICAL REPRINTS:** Information derived from NASA activities and initially published in the form of journal articles.

**SPECIAL PUBLICATIONS:** Information derived from or of value to NASA activities but not necessarily reporting the results of individual NASA-programmed scientific efforts. Publications include conference proceedings, monographs, data compilations, handbooks, sourcebooks, and special bibliographies.

*Details on the availability of these publications may be obtained from:*

**SCIENTIFIC AND TECHNICAL INFORMATION DIVISION**

**NATIONAL AERONAUTICS AND SPACE ADMINISTRATION**

**Washington, D.C. 20546**